Stable carbon isotope systematics of methane, ethane and propane from low-permeability hydrocarbon reservoirs

Jaime Cesar[a,*], *Michael Nightingale*[a], *Veith Becker*[a], *and Bernhard Mayer*[a]

[a]Department of Geoscience, University of Calgary, 2500 University Drive, Calgary, Alberta, T2N 1N4, Canada

*Corresponding author: jaimerafael.cesarcol@ucalgary.ca

Corresponding author present address: Natural Resources Canada, Geological Survey of Canada, 3303 33rd St. NW Calgary, AB, T2L 2A7, Canada

Abstract

We have reassessed the stable carbon isotope systematics of methane (C_1), ethane (C_2), and propane (C_3) in more than 500 natural gas samples from low-permeability hydrocarbon reservoirs around the world, with the purpose of providing new tools for thermal maturity assessment of natural gas that is increasingly produced from such reservoir types world-wide. A low-permeability reservoir resembles a semi-closed system and we found that the stable carbon isotope distribution in C_1-C_3 alkanes differs partially from what has been previously observed in natural gas from conventional hydrocarbon accumulations (e.g. C isotope distributions dominated by Rayleigh distillation and kinetic isotope effects). In a low-permeability reservoir, isotope exchange may play a more prominant role in the carbon isotope distribution, driving the system towards an even isotopic distribution (EID) of 6 ‰ between methane and ethane, and ethane and propane, at R_o of 1.5 %. At higher maturity, ethane and propane depleted in ^{13}C are formed as a consequence of thermal cracking of wet-gas components and possibly free radical decomposition/polymerization reactions, which leads to the occurrence of isotope reversals ($\delta^{13}C_{C_2} < \delta^{13}C_{C_1} < \delta^{13}C_{C_3}$, $\delta^{13}C_{C_2} < \delta^{13}C_{C_3} < \delta^{13}C_{C_1}$ and $\delta^{13}C_{C_3} < \delta^{13}C_{C_2} < \delta^{13}C_{C_1}$) at thermal maturity higher than 2.0 $\%R_o$. The diagram of the isotopic differences $\Delta^{13}C_{C_1\text{-}C_2}$ ($\delta^{13}C_{C_1} - \delta^{13}C_{C_2}$) versus $\Delta^{13}C_{C_1\text{-}C_3}$ ($\delta^{13}C_{C_1} - \delta^{13}C_{C_3}$) provides a new tool for classification of natural gas from low-permeability hydrocarbon reservoirs according to thermal history in three main regions: normal trend (subdivided into immature, oil/wet-gas window, and dry gas window), ethane reversal, and propane reversal with respect to methane. This new tool can be used to assess the maturity of the petroleum fluids and can assist in identifying hydrocarbon mixing.

Keywords: gas; carbon; isotope; low-permeability; unconventional; reversal

1- Introduction

Over several decades of conventional hydrocarbon exploration, efforts have been made to characterize natural gas of different origins using chemical and isotopic techniques. The main challenge, as explained by Schoell (1983), has been the identification of multiple geochemical processes that result in the formation

of natural gas, including (i) bacterial degradation of organic matter in immature sediments, (ii) thermal degradation of kerogen, and (iii) thermal degradation of crude oil; from post-generation processes that include (i) migration, (ii) hydrocarbon mixing, and (iii) methane oxidation by bacteria. Schoell (1983) provided graphical tools based on molecular and isotopic data for the genetic characterization of natural gas, but emphasized that absolute boundaries do not exist between geochemical properties of gases from different sources.

Since then, compound specific isotope analysis (CSIA) of natural gas has emerged as a powerful tool in identifying the source of organic matter as well as the thermal history of generated hydrocarbons in conventional accumulations of petroleum. For example, Chung et al. (1988) proved that the stable carbon isotope ratio of *n*-alkane gases (C_1-C_5) increases with carbon number, and that the linear relationship between the carbon isotope values and the reciprocal of carbon number can indicate the carbon (C) isotopic composition of the original kerogen. This assumes that the source possesses a homogeneous C isotopic composition, and that there was only one thermal cracking event. Several exceptions to the scenario proposed by Chung et al. (1988) have been reported because the original organic matter is not always homogeneous, and some alteration processes (*e.g.* thermochemical sulphate reduction or TSR) can take place (Zou et al., 2007; Liu Q. et al., 2019). Also, Faber (1987) proposed a logarithmic relationship between the isotopic composition of C_1-C_3 and the vitrinite reflectance of the source rock for gases from sapropelic kerogen. Interest in the stable carbon isotope systematics of methane, ethane and propane continued with focus on isotopic fractionation mechanisms as a function of thermal maturity, and several mathematical models were proposed for gas mixing scenarios (e.g. Berner and Faber, 1988; Whiticar, 1994).

In 1991, Clayton demonstrated that changes in the isotopic composition of C_1-C_3 alkanes from kerogen (1991b) and oil (1991a) in conventional hydrocarbon reservoirs can be modelled as a Rayleigh distillation process. In this model, the isotopic fractionation occurs under normal kinetic isotope effects as the reaction rate of compounds comprising weaker bonds (e.g. ^{12}C-^{12}C bonds) is higher than that of compounds with bonds formed with the heavy isotope ^{13}C. Therefore, the product becomes enriched in ^{12}C compared to the remaining source material. The models by Clayton (1991a, b) allowed for gas accumulation and described the isotope ratios of the accumulated gas, however, the principle of a Rayleigh distillation implies that the generated gas does not remain in contact with parental organic matter.

The extent of kinetic isotope effects depends on the reaction yield, i.e. the distribution of material (Kaye, 1992). This implies that the Rayleigh model will vary according to the source of hydrocarbons. In fact, Clayton (1991a) proposed a model for labile kerogen (sapropelic sources) and another model for refractory kerogen (humic sources). This dependence on the source of organic matter has been largely confirmed in a variety of subsequent kinetic fractionation models for different kerogen types (*e.g.* Berner et al., 1995; Rooney et al., 1995; Berner and Faber, 1996; Whiticar, 1999; Tang et al., 2000; Li et al., 2008). Overall, different basins will have distinct kinetic models for stable carbon isotope fractionation, which depend on the source of organic matter and the hydrocarbons accumulation history (Li et al., 2008).

Lorant et al. (1998) introduced the residence time as another key factor controlling isotopic fractionation of generated gases in conventional hydrocarbon reservoirs. In such systems, the source rocks are open systems where natural gas has a low residence time in the source rock compared to its generation rate

(Lorant et al., 1998), since it resides predominantly in the physically distant hydrocarbon trap after gas migration.

Interestingly, with the development of unconventional hydrocarbon resources (including low-permeability reservoirs) commencing at the beginning of the 21st century, the isotopic tools that resulted from many years of conventional hydrocarbon exploration continued to be applied, without much reconsideration. The same concepts of isotopic fractionation have been adopted although they were conceived for a Rayleigh distillation process that involved continuous removal of material from the system, which is not the case in a tight source-rock/reservoirs and other low-permeability hydrocarbon reservoirs containing fluids that migrated at most very short distances. Current genetic diagrams for natural gases are rather complex, with significant overlap of gases from different origins and formation mechanisms, and do not make distinction between gases from conventional and unconventional hydrocarbon reservoirs (Milkov and Etiope, 2018). In this study, we use the term low-permeability reservoir (e.g. typically shales, siltstones, or tight sandstones) referring to reservoirs that require hydraulic fracturing to produce hydrocarbons. These include (i) source rocks that also act as reservoirs (locally derived hydrocarbons), (ii) reservoirs containing hydrocarbon that migrated relatively short distances from the source, and (iii) reservoirs that trapped migrated hydrocarbons before their further burial and maturation (usually during late diagenesis), thus implying further thermal alteration of the migrated hydrocarbons.

In low-permeability reservoirs, a common exception to the Rayleigh models includes the isotope reversal phenomenon, which consists of ethane and propane having more negative $\delta^{13}C$ values compared to methane (*e.g.* Burrus and Laughrey, 2010; Tilley et al., 2011; Zumberge et al., 2012; Chatellier et al., 2013; Tilley and Muehlenbachs, 2013; Gao, 2016; Faiz et al., 2018). A persistent explanation for carbon isotope reversals suggests mixing of low maturity fluids with high maturity fluids, which others refer to as the mixing of kerogen-cracked and secondary oil-cracked alkane gases (*e.g.* Hao and Zou, 2013; Xia et al., 2012; Dai et al., 2016; Zhang S. et al., 2018). Other studies indicate that the occurrence of isotope reversals requires the presence of water to proceed under specific chemical reactions (Burrus and Laughrey, 2010; Zumberge et al., 2012; Gao et al., 2014; Qu et al., 2016) although it has been demonstrated during pyrolysis experiments that water is not necessary for the C isotope reversal to occur if the temperature is raised to over 500 °C (Ni et al., 2018).

Recent research suggests that the occurrence of C isotope reversals might not be always related to the productivity of the shale (*e.g.* Wu et al., 2019). Instead, the formation of ^{12}C enriched ethane and propane could be associated with a series of chemical reactions in highly-mature shales due to the instability of some select hydrocarbon compounds. These reactions may involve abiogenic polymerization of methane (Zeng et al., 2013), demethylation of mono-aromatic compounds and subsequent reaction between methyl radicals (Mi et al., 2018), and partly reversible reactions that include the formation of ethyl and propyl radicals and cations, which reversibly form ethane and propane associated with kinetic C isotope effects (Xia and Gao, 2018).

The objective of this paper is to re-assess the carbon isotope systematics of methane, ethane and propane from several low-permeability hydrocarbon reservoirs world-wide, with the goal of distinguishing natural gas samples at different stages of thermal history, including (i) low-maturity, (ii) oil/wet-gas window, and (iii) dry gas window. We describe the C isotope distribution of methane, ethane and propane applicable to low-permeability reservoirs, and suggest chemical and isotopic pathways that result in the observed C

isotope patterns. This new tool can be used to assess the maturity of the petroleum fluids and can assist in identifying hydrocarbon mixing. The goals are achieved by interpreting compositional and carbon isotope data for more than 500 samples from low-permeability hydrocarbon reservoirs around the world. We also apply the developed concepts to our own data set for samples from the Montney Formation, the most productive tight hydrocarbon play in Canada (National Energy Board, 2013) and a major shale gas play worldwide.

2- Study Sites

For this study, we reviewed and reinterpreted previously published compositional data and stable carbon isotope ratios ($\delta^{13}C$) for hydrocarbon plays in various countries, and obtained samples from the Montney Formation in Western Canada for subsequent chemical and isotopic analyses.

The Montney depositional fairway extends over 88,500 km^2 from Northeast British Columbia to Northwest Alberta (Figure 1), in the Western Canadian Sedimentary Basin (WCSB). The formation is a sedimentary wedge that dips from the northeast to the southwest, and its thickness varies from less than 1 m (easterly sub-crop) to over 350 m in the west. The Montney Fm. is unconformable overlain by Triassic to Cretaceous sediments (west to east), and conformably overlies the Permian Belloy Formation (Kuppe et al., 2012).

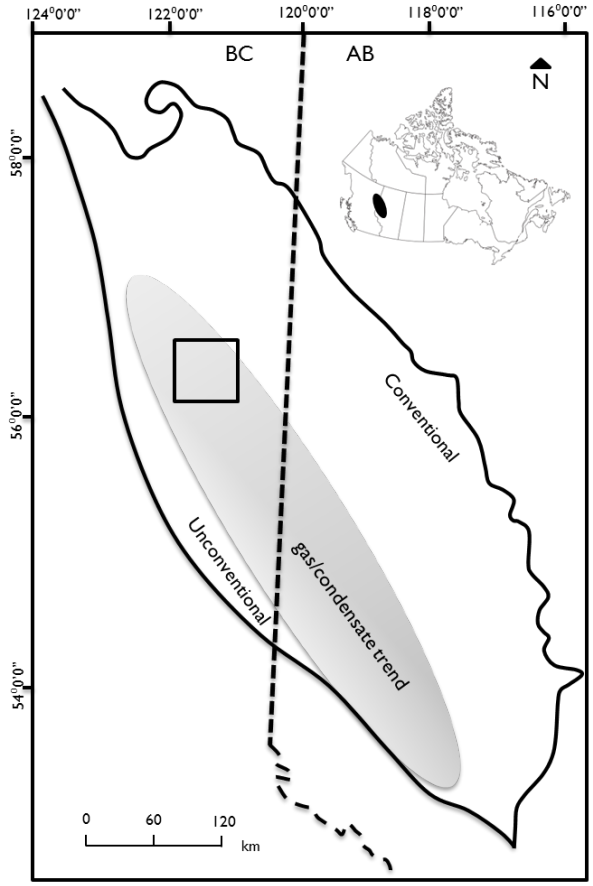

Figure 1. The location of the Montney Formation in Western Canada, its resource types, and the study area (rectangle). Modified after the National Energy Board (2013).

The Montney Formation accumulated type II/III kerogen, with an average total organic carbon content (TOC) of 1.5 % from northwestern Alberta to northeastern British Columbia (Riediger, 1990, 1997; Ibrahimbas and Riediger, 2004). Egbobawaye (2017) also found kerogen types IV and III/IV in the British Columbia section, and reported an overall good organic matter enrichment that reaches a TOC content of 3.5 %. The Montney Formation is within the oil window, and is more mature in British Columbia than in Alberta (with some exceptions, Riediger, 1990). The general maturity trend follows a NE-SW direction (BC Oil and Gas Commission, 2012; Rokosh et al., 2012; Ferri et al., 2013; Egbobawaye, 2017).

We have analyzed a total of 36 mud-gas samples obtained in IsoTubes from the Montney Formation, from a well in British Columbia (well A), covering an interval of 200 meters in the vertical section, and landing in the Lower Member of the Montney Formation at a depth of 2.5 km (Table S1). The mud-gas isotope logging (MGIL) represents a sampling and analytical technique that enables the molecular and isotopic analysis of air-contaminated hydrocarbon gases that are collected from the circulating mud stream during drilling (Ellis et al., 2003).

In addition, we accessed previously published data for gas samples from various low-permeability hydrocarbon reservoirs around the world as described in Tables 1, S2 and S3. Detailed explanations are provided using the stable carbon isotope distributions versus depth first reported by Chatellier et al. (2013) based on mud-gas IsoJar samples from the Ordovician Lorraine Shale, in the St. Lawrence Lowlands, Quebec, Canada (Table S2). The Lorraine Shale is a flysch succession dominated by mudstones and siltstones with local thicker bedded sandstones (Lavoie et al., 2011). This dataset (Table S2) is of great value because of a suitable sampling density within an approximately 1.5 km depth profile and a wide thermal maturity range from ≈0.6 to ≈2.0 %R_o (Chatellier et al., 2013). The other study sites are described in 19 published studies conducted for low-permeability hydrocarbon reservoirs in Canada, USA, China, Saudi Arabia, Poland and Australia, summarized in **Table 1**. The carbon isotope data for C_1 to C_3 for samples from these studies were reinterpreted in concert with additional information regarding source-rock and reservoir type, thermal maturity as vitrinite reflectance (R_o) when known, and prominent lithofacies. The majority of the samples were sampled as produced gas near the well head, while in some cases mud-gas was collected in IsoTubes, or hydrocarbon gases were collected after outgassing of cuttings or core (**Table S3**). It is recognized that the usage of different sampling approaches introduces an additional variability into the compiled data set, but we postulate that the variations in data patters observed and interpreted below far exceed those introduced by slightly variable sampling approaches. Additional information about these reservoirs and the sampling approaches can be found in the supplementary material.

174

175

176

177 **Table 1**. Source of the gas isotope data used in this paper. *: maturity estimated using bitumen reflectance
178 or carbon isotope regression. nr: not reported.

Country	Source-rock / reservoir	Lithofacies	Approximate % R_o	Reference
Canada	Montney Fm.	Siltstone	nr	Tilley and Muehlenbachs (2006)
			nr	Tilley and Muehlenbachs (2013)
			0.9-1.3	Sereda (2017)
			nr	Chatellier et al. (2018)
	Doig Fm.	Siltstone	nr	Tilley and Muehlenbachs (2013)
	Horn River Shale	Shale	nr	
	Pardonet/Baldonnel Fm.	Limestone/dolomite	nr	Tilley et al. (2011)
	Belcourt Fm.	Limestone/siltstone	nr	
	Charlie Lake Fm.	Limestone and dolomitic siltstone and sandstone	nr	
	Mannville Group	Sandstone with interbedded siltstone and shale	0.3-0.4	Rowe and Muehlenbachs (1999)
USA	Barnett Shale	Shale	1-2	Zumberge et al. (2012)
	Fayetteville Shale	Shale	2-3	
	Clinton/Medina Group	Sandstone	1.5-3	Repetski et al. (2008); Burrus and Laughrey (2010)
	Black River Fm.	Limestone	>3	
	Woodford Shale	Shale	1-1.6	Liu C. et al. (2019)
China	Longmaxi Fm.	Marine shale	2.7-3.3	Gao (2016); Zhang S. et al. (2018)
	Wufeng-Longmaxi	Shale	2.2-3.13	Dai et al. (2016)
	Shanxi/Benxi Fm.	Sandstone	>2.4	
	Yanchang Fm.	Lacustrine shale	<0.9	Fan et al. (2018)
Saudi Arabia	Hanifa Fm.	Limestone	1-1.5* (this maturity will be reassessed in this paper)	Hakami et al. (2016)
	Tuwaiq Mnt Fm.	Limestone		
	Jubaila	Limestone		
Poland	Eastern Pomeranian	Sandstone	Oil window	Kotarba and Nagao (2015)
	Western Pomeranian	Sandstone	1.5-2*	
	Baltic Basin	Shale	nr	Janiga et al. (2015)
Australia	Velkerri Fm.	Shale	Tmax 542 °C	Faiz et al. (2018)
	Toolebuc Fm.	Calcareous mudstone	0.6-1.2	Troup et al. (2018)

179

3- Methods

3.1 The C_1-C_5 molecular composition by gas chromatography — flame-ionization detection (GC-FID)

A total of 36 gas samples collected in IsoTubes from a well drilled in Northeast British Columbia (see study area in **Figure 1**) were analyzed, as well as a produced gas sample from the wellhead of the same well, and five other produced gas samples from the Montney Formation. For molecular analysis, a 5 mL aliquot of gas was removed from each IsoTube/gas-cylinder via a modified IsoTube/gas-cylinder septum valve and locking gas-tight syringe. Gas compositional analysis (C_1 to C_5 alkanes) was completed by injecting the sample into a Scion 450/456 gas chromatograph (GC). The GC utilizes four separate analytical columns connected to three thermal conductivity detectors and a flame-ionization detector for gas separation and quantification. The lower detection limit for hydrocarbons is 1 ppm. Certified gas standards were used to calibrate the GC immediately prior to the analysis. Analytical drift was monitored by injecting the appropriate gas standards after every ten samples analyzed. Analytical precision and accuracy for gas composition analysis is typically better than ± 2.5% of the reported concentrations of methane, ethane and propane.

3.2 Compound Specific Isotope Analysis (CSIA) of natural gas by gas chromatography — isotope ratio mass spectrometry (GC-irMS)

The compound specific $\delta^{13}C$ values of C_1 to C_3 alkanes were determined using continuous flow isotope ratio mass spectrometry. The system is comprised of a Thermo Trace GC – GC-IsoLink system interfaced to a Thermo MAT 253 mass spectrometer via a Thermo Conflo IV. Gas sampling was conducted as indicated above for GC compositional analysis. Aliquots of gas were injected into a helium carrier stream through the inlet of the GC using a gas tight syringe. Air, carbon dioxide (CO_2) and the hydrocarbon compounds of the gas were separated on a GC column before passing through a combustion reactor maintained at 1030 °C. All hydrocarbon gas species were quantitatively converted to CO_2 by passing the sample gas mixture through the combustion furnace. The separate CO_2 gas pulses were then swept sequentially, by the carrier gas, through a water trap (Nafion®) then into the open split interface which facilitates steady continuous flow of the gas into the mass spectrometer. Final sample carbon isotope ratios were normalized and calculated using a 2-point calibration (linear regression) against specially prepared *AirLiquide Alphagaz*® calibration standards analyzed typically at the beginning and end of each workday, which cover the $\delta^{13}C$ range of the gas samples. The $\delta^{13}C$ values of the unknown species were determined using the instrument software (ISODAT 3.0) and are expressed in the usual per mil notation (‰) relative to the international V-PDB standard, with an uncertainty of 0.5 ‰.

3.3 Stable carbon isotopes dataset and data treatment

In addition to measurements on our samples obtained from the Montney reservoir, a database with stable carbon isotope ratios ($\delta^{13}C$) of C_1-C_3 gas from low-permeability hydrocarbon reservoirs around the world has been constructed (Table S3). This database is comprised of $\delta^{13}C$ values of methane, ethane, and propane in produced gas and some mud-gas samples from plays in Canada, China, USA, Saudi Arabia, Poland and Australia. The analytical procedures used in these studies can be found in the corresponding references given in Table 1.

In this paper, the diagrams presented in Figures 2-6 and 8-11 are based on the difference between $\delta^{13}C$ values of C_1, C_2, and C_3, denoted as $\Delta^{13}C$, instead of the individual $\delta^{13}C$ values. The individual $\delta^{13}C$ values preserve a source signature, especially during early maturity, whereas the $\delta^{13}C$ difference between two compounds is controlled by thermal maturity (James, 1983; Prinzhofer and Huc, 1995; Rooney et al., 1995). Gai et al. (2019) suggested that the isotopic difference between compounds is not affected by retained bitumen in the source rock. The reported $\Delta^{13}C$ values will include the difference between the $\delta^{13}C$ of methane and ethane ($\Delta^{13}C_{C_1\text{-}C_2}$), the difference between $\delta^{13}C$ of methane and propane ($\Delta^{13}C_{C_1\text{-}C_3}$), and the difference between the $\delta^{13}C$ of ethane and propane ($\Delta^{13}C_{C_2\text{-}C_3}$). The $\Delta^{13}C$ values will carry a greater uncertainty than the individual $\delta^{13}C$ (around +/-0.7 ‰ as the individual $\delta^{13}C$ values typically report +/-0.5 ‰), and this is due to propagation of uncertainty. However, we will exclusively refer to changes exceeding ±1 ‰ which are considered statistically significant.

4- Results

4.1 Depth trends of stable carbon isotope distribution of C_1-C_3 alkanes from a low-permeability reservoir

In order to interpret trends of carbon isotope ratios with depth we have chosen the example of four vertical wells completed in the Lorraine Shale (Quebec, Canada) using data reported by Chatellier et al. (2013). Figures 2a-d display the trends of $\delta^{13}C$ values of methane, ethane and propane with increasing depth. $\delta^{13}C$ values of methane are generally most negative (circa -45 ‰) during the first 400 m TVD (true vertical depth) and subsequently increase towards -40 ‰ with increasing depth. The $\delta^{13}C$ values of ethane and propane also initially increase with increasing depth from approximately -37 to -34 ‰, and -33 to -27 ‰, respectively. However, at a depth between 1500 and 1800 m (depending on the well), the $\delta^{13}C$ values of ethane and propane start to decrease with increasing depth (Figures 2a-d), approaching $\delta^{13}C$ values similar or even more negative than those of methane. While the $\delta^{13}C$ values of ethane and propane become more negative, the $\delta^{13}C$ of methane continues to increase slightly or remains constant.

Inspection of the $\Delta^{13}C$ depth profiles for samples from the Lorraine Shale (Quebec, Canada) reveals that $\Delta^{13}C_{C_1\text{-}C_2}$ values in the upper portion of the profile consistently range between -7 and -14 ‰, indicating a large difference between $\delta^{13}C$ of methane and ethane to depths of approximately 1500 m. In contrast, $\Delta^{13}C_{C_2\text{-}C_3}$ values display much smaller differences in $\delta^{13}C$ values of ethane and propane consistently ranging between -3 and -7 ‰ in the upper portions of the profiles (**Figures 2e-h**). In this same section, $\Delta^{13}C_{C_1\text{-}C_3}$ values range between -11 and -20 ‰.

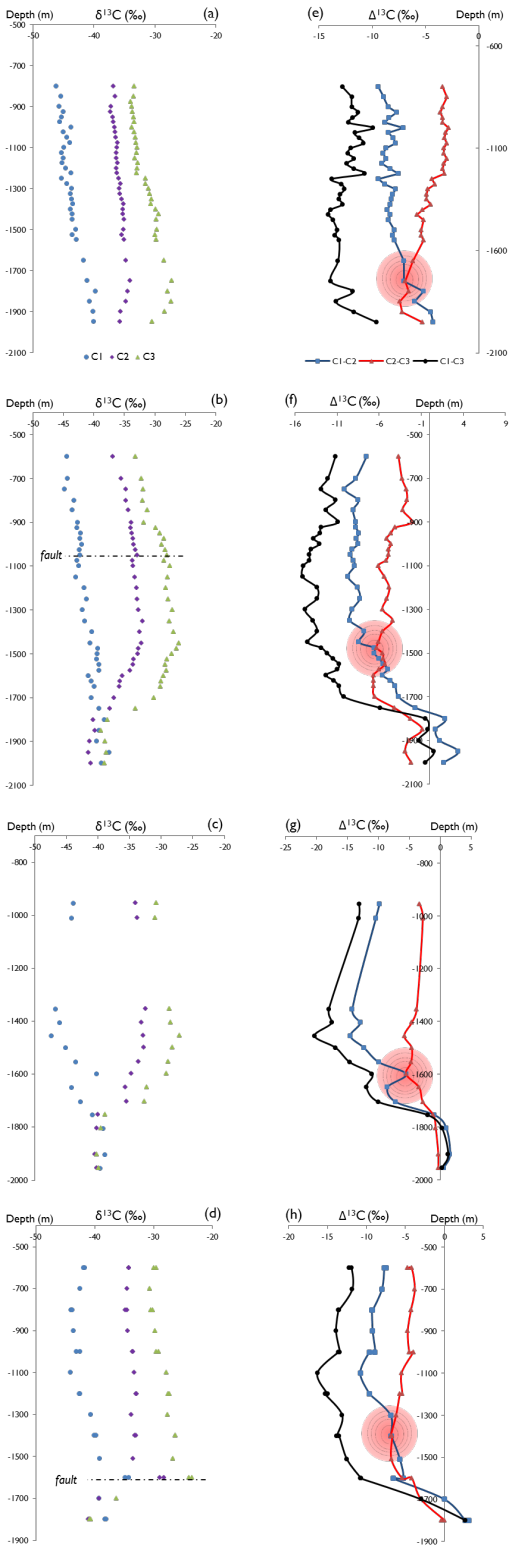

Figure 2. Methane, ethane and propane $\delta^{13}C$ profiles (a-d) and the corresponding $\Delta^{13}C_{C_1\text{-}C_2}$, $\Delta^{13}C_{C_2\text{-}C_3}$, and $\Delta^{13}C_{C_1\text{-}C_3}$ values (e-h) of samples from four wells from the Lorraine Shale, Quebec. Data from Chatellier et al. (2013). The wells are a,e) Fortierville, b,f) Leclercville, c,g) St. Edouard 1a, and d,h) St. Edouard 1.

In the lower portion of the profile, $\Delta^{13}C_{C_1\text{-}C_2}$ and $\Delta^{13}C_{C_2\text{-}C_3}$ values start to converge and approach similar values of -6 ± 1 ‰ (see red dots in Figures 2e-h). Here, the difference between the $\delta^{13}C$ values of methane and ethane equals the difference between the $\delta^{13}C$ values of ethane and propane, a situation referred to as even-isotopic-distribution (EID). After this crossing point, the $\delta^{13}C$ values of ethane and propane start to decrease with increasing depth (Figures 2a-d).

With further depth, $\Delta^{13}C_{C_1\text{-}C_2}$ values show an increasing trend from -6 ± 1 ‰ progressing towards 0 ‰ (Figures 2e-h). The $\Delta^{13}C_{C_2\text{-}C_3}$ continues to decrease below -6 ‰ for about 100 m after the EID and subsequently shifts to an increasing trend also progressing towards 0 ‰ (Figures 2e-h). In three of the four wells, $\Delta^{13}C_{C_1\text{-}C_2}$ values become positive revealing the occurrence of an ethane isotope reversal, where the $\delta^{13}C$ of ethane has become more negative than the $\delta^{13}C$ value of methane (Figures 2f-h). The $\Delta^{13}C_{C_2\text{-}C_3}$ value approaches 0 ‰ in two of the four wells (Figures 2g,h) indicating that $\delta^{13}C$ values of ethane and propane converge to similar values but propane is not yet in isotope reversal with respect to ethane. The $\Delta^{13}C_{C_1\text{-}C_3}$ values also tend towards zero and even positive values, indicating isotope reversal of propane with respect to methane.

4.2 Thermal maturity indicators and their relation to gas composition and carbon isotope ratios of C_1-C_3 alkanes for a low-permeability reservoir

Thermal maturity determinations on rock samples from a nearby well indicate that thermal maturity increases with depth ranging from 0.6 $\%R_o$ in the shallower sections to 2.0 %Ro in the deepest part of the reservoir accessed by these wells (Heroux and Bertrand, 1991; Chatellier et al., 2013).

To investigate and illustrate how changes in reservoir maturity affect the gas composition and the $\delta^{13}C$ values of C_1-C_3 alkanes with increasing depth, we have chosen parameters for two vertical wells completed in the Lorraine Shale (Quebec, Canada) using data reported by Chatellier et al. (2013) with results summarized in Figure 3.

The *iso*-butane to butane ratio (iC_4/nC_4) is a parameter that has been found to increase with maturity during the oil to early/middle gas generation windows (e.g. Hao and Zou, 2013). This ratio decreases at higher thermal maturity due the increasing importance of wet-gas cracking (relative to kerogen cracking), a process that generates more *n*-C_4, and later destroys both compounds (Hao and Zou, 2013). Hence the iC_4/nC_4 ratio has been found to constitute a highly consistent and reliable maturity indicator in shale gas samples (e.g. Zumberge et al., 2012; Wood and Sanei, 2016). Chatellier et al. (2013) found that the initially increasing trend of iC_4/nC_4 in the upper portions of the wells shifts abruptly to low values at the same depth where ^{13}C depletion of ethane and propane takes place. This shift of the iC_4/nC_4 ratio identified in gas hydrocarbons and the onset of the decreasing trend of this parameter has been proposed to occur at circa 1.5 % R_o (e.g. Zumberge et al., 2012; Chatellier et al., 2013; Xia et al., 2012). Figures 3c,d illustrate this phenomenon and further reveal that the *iso*-butane to butane ratio starts to decrease where the carbon isotope ratios first reach an even-isotopic-distribution (EID) (Figure 3a,b).

Zumberge et al. (2012) as well as Tilley and Muehlenbachs (2013) found that the occurrence of isotope reversal was associated with low-permeability reservoirs containing dry gas. We illustrate this by displaying the depth trends of the relative abundance of methane, ethane and propane (in mol %) for the two selected

295 wells in Figures 3e,f. In the upper portion of the profiles, methane is the predominant hydrocarbon
296 compound while ethane and propane occur at lower but similar concentrations. With increasing depth
297 and as carbon isotope ratios approach EID (Figures 3a,b; yellow highlighted zone in Figure 3) the gas
298 becomes progressively drier as reflected by the increasing abundance of methane (Figures 3ef), while the
299 relative abundance of ethane and propane decreases continuously. It is also noteworthy that the ethane
300 to propane ratio (C_2/C_3), which was close to 1 in the upper part of the two profiles, markedly increases
301 to values between 4 and 16 (Figure 3g,h) in the lower portion of these wells where EID was observed.

302 Figures 3i-l display the trends in $\delta^{13}C$ values of ethane and propane with relation to the above mentioned
303 parameters. In the upper portion of the wells, $\delta^{13}C$ values of ethane and propane progressively increase
304 with increasing depth by 4 to 6 ‰. As soon as EID conditions are reached (e.g. yellow highlighted zone in
305 Figure 3) and the iC_4/nC_4 ratio starts to decrease, the $\delta^{13}C$ values of ethane and propane progressively
306 decrease (Figures 3i-l). In the Leclerville shale gas well the $\delta^{13}C$ values of ethane decrease by 8 ‰ (Figure
307 3j) and the $\delta^{13}C$ values of propane decrease by 12 ‰ (Figure 3l). The $\delta^{13}C$ value of methane continues to
308 increase after the EID in these two wells (Figure S1).

309 The trends described here using data from Chatellier et al. (2013) for two wells completed in the Lorraine
310 Shale (Quebec, Canada) clearly suggest that increasing maturity is associated with the occurrence of EID,
311 the evolution towards drier shale gas, and a trend towards carbon isotope reversal of ethane with respect
312 to methane, and of propane with respect to methane and ethane.

313

314

315

316

317

318

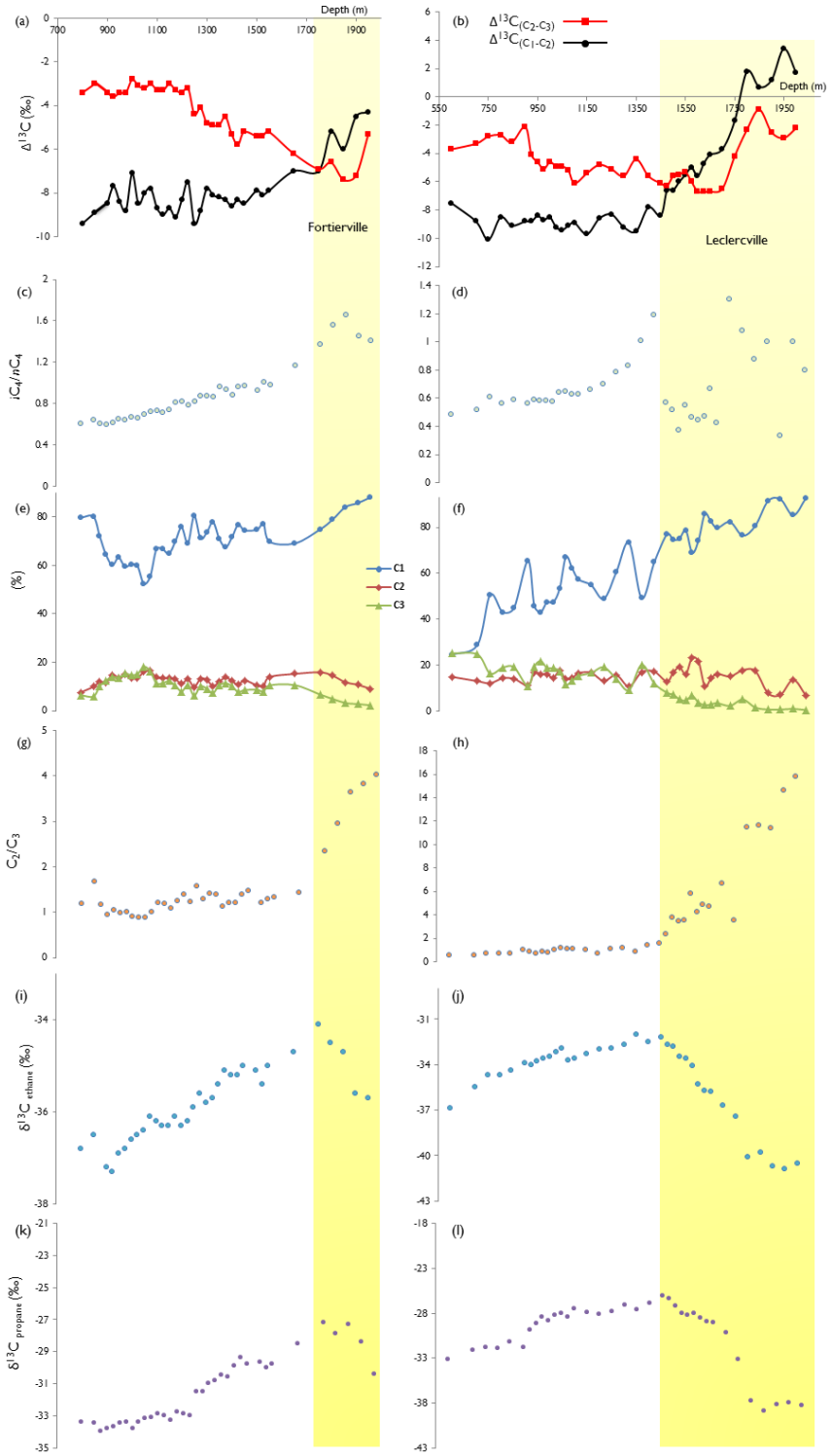

Figure 3. Molecular and isotopic changes with increasing depth before and after the even isotopic distribution (EID) for samples from the wells (a) Fortierville and (b) Leclercville from the Lorraine shale, as indicated by: (c,d) the *iso*-butane to *n*-butane ratio iC_4/nC_4, (e,f) % mole distribution of C_1-C_3 alkanes as reported by Chatellier et al. (2013), (g,h) the C_2/C_3 ratio, (i,j) the $\delta^{13}C$ of ethane, and (k,l) the $\delta^{13}C$ of propane.

4.3 The $\Delta^{13}C_{C_1\text{-}C_2}$ versus $\Delta^{13}C_{C_1\text{-}C_3}$ plot and its relation to thermal maturity

To test whether the patterns revealed above also apply to other shale gas reservoirs around the world (Table 1), we further investigated the evolution of stable carbon isotope ratios of ethane and propane with respect to methane, and thus the dependence of $\Delta^{13}C_{C_1\text{-}C_2}$ and $\Delta^{13}C_{C_1\text{-}C_3}$ values on thermal maturity as indicated by literature data.

In Figure 4, the $\Delta^{13}C_{C_1\text{-}C_2}$ value is plotted versus the $\Delta^{13}C_{C_1\text{-}C_3}$ value for gas samples from shale gas reservoirs in Canada, USA, China, Saudi Arabia, Poland and Australia (see Table 1). All data fall near a straight line. Samples from the Mannville Group (Canada) and the Jafurah Basin (Saudi Arabia) exhibit the most negative $\Delta^{13}C_{C_1\text{-}C_2}$ and $\Delta^{13}C_{C_1\text{-}C_3}$ values of <-18 ‰ and <-23 ‰, and display a linear increasing relationship. Samples from the Barnett, Woodford (USA), and Lorraine (Canada) shales are characterized by $\Delta^{13}C_{C_1\text{-}C_2}$ values ranging between -15 and 0 ‰ and by $\Delta^{13}C_{C_1\text{-}C_3}$ values varying between -20 and -6 ‰ while displaying a linearly increasing trend at a ~1:1 ratio (correlation coefficient of 0.73). Samples from reservoirs in China, the Fayetteville Shale (USA), and other plays in the Western Canadian Sedimentary Basins (e.g. Doig, Horn River, and Charlie Lake formations) plot on the top right corner of Figure 4, with positive $\Delta^{13}C_{C_1\text{-}C_2}$ values and $\Delta^{13}C_{C_1\text{-}C_3}$ values of up to 10 ‰.

The known maturity of the reservoirs (based on vitrinite reflectance data) has been used to define the maturity windows shown on the $\Delta^{13}C_{C_1\text{-}C_2}$ versus $\Delta^{13}C_{C_1\text{-}C_3}$ plot (Figure 4) since the distribution of the isotope data appears to be predominantly governed by the maturity of the hydrocarbon reservoirs. For example, as shown in Table 1, the Lacustrine Yanchang Shale from China has been reported to be immature (<0.8 $\%R_o$, Fan et al., 2018) and samples from the Toolebuc Formation, Australia, have $\%R_o$ between 0.5 to 1.2 (Troup et al., 2018) whereas samples from the Mannville Group correspond to a maturity of 0.4 $\%R_o$ (Rowe and Muehlenbachs, 1999). Samples from these reservoirs are characterized by the most negative $\Delta^{13}C_{C_1\text{-}C_2}$ and $\Delta^{13}C_{C_1\text{-}C_3}$ values in Figure 4. In contrast, the Barnett Shale has reached the oil window with thermal maturities varying from 1.0 to 2.0 of $\%R_o$ (Zumberge et al., 2012), and the $\Delta^{13}C_{C_1\text{-}C_2}$ and $\Delta^{13}C_{C_1\text{-}C_3}$ values of its gas are considerably less negative (>-15 ‰ and >-20 ‰, respectively). The maturity in the Clinton/Medina Group ranges from 1.5 to 3.0 $\%R_o$ (Repetski et al., 2008) and the Longmaxi Formation in China is highly mature with a $\%R_o$ ranging between 2.7 and 3.3 % (Feng et al., 2017). Gas samples from these two reservoirs are characterized by the most positive $\Delta^{13}C_{C_1\text{-}C_2}$ and $\Delta^{13}C_{C_1\text{-}C_3}$ values ($\Delta^{13}C>0$).

We observe that the plot distributes the data into three quadrants with increasing maturity. These contain (i) samples with normal trend $\delta^{13}C_{C_1} < \delta^{13}C_{C_2} < \delta^{13}C_{C_3}$ ($\Delta^{13}C_{C_1\text{-}C_2}$ and $\Delta^{13}C_{C_1\text{-}C_3}$ are both negative) and low to intermediate reservoir maturity (subdivided into immature, oil/wet-gas window, and wet-gas to dry gas window), (ii) samples in ethane reversal $\delta^{13}C_{C_2} < \delta^{13}C_{C_1} < \delta^{13}C_{C_3}$ ($\Delta^{13}C_{C_1\text{-}C_2}$ is positive and $\Delta^{13}C_{C_1\text{-}C_3}$ is negative) and very high reservoir maturity, and (iii) samples in propane isotope reversal with respect to methane, $\delta^{13}C_{C_3} < \delta^{13}C_{C_2} < \delta^{13}C_{C_1}$ or $\delta^{13}C_{C_2} < \delta^{13}C_{C_3} < \delta^{13}C_{C_1}$ ($\Delta^{13}C_{C_1\text{-}C_2}$ and $\Delta^{13}C_{C_1\text{-}C_3}$ are both positive), having the most extreme reservoir maturity.

The EID of 6 ‰ is associated with a thermal maturity of 1.5 $\%R_o$ (see red highlight in Figure 4) indicating a reservoir maturity at which key geochemical changes take place as described in section 4.2 that include a trend of decreasing $\delta^{13}C$ values of ethane and propane.

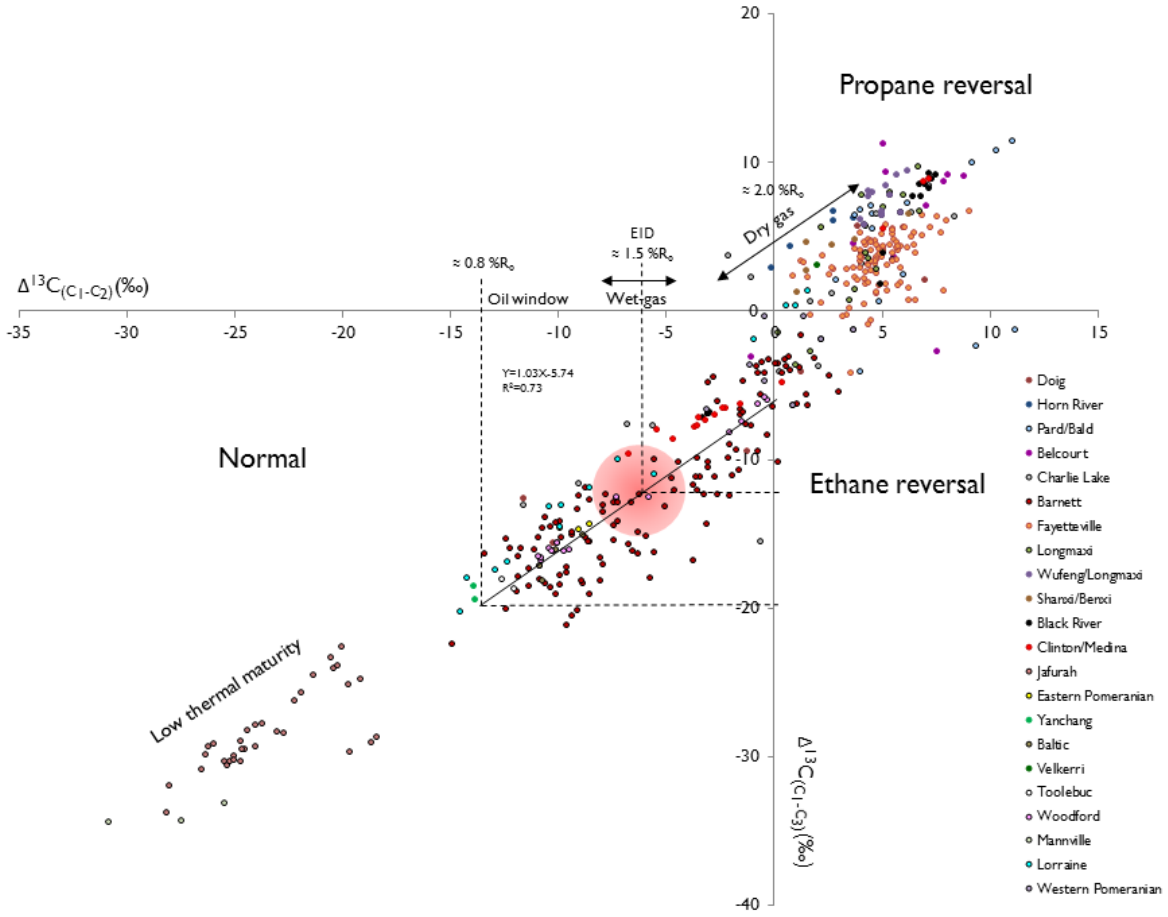

Figure 4. The $\Delta^{13}C_{C_1\text{-}C_2}$ versus $\Delta^{13}C_{C_1\text{-}C_3}$ plot for gas classification. Gas samples from low-permeability reservoirs around the world.

4.4. Stable carbon isotope database from the Montney Formation, WCSB

We have also compiled $\delta^{13}C$ values of methane, ethane and propane for gas samples from the unconventional portion of the Montney Formation (Canada), available in the literature as well as those measured in our laboratory (see also Tables 1 and S1). On the $\Delta^{13}C_{C_1\text{-}C_2}$ versus $\Delta^{13}C_{C_1\text{-}C_3}$ plot (Figure 5), these samples range from -19 to -7 ‰ for $\Delta^{13}C_{C_1\text{-}C_2}$, and from -23 to -10 ‰ for $\Delta^{13}C_{C_1\text{-}C_3}$ with only two samples deviating from the linear trend with $\Delta^{13}C_{C_1\text{-}C_2}$ > -5 ‰.

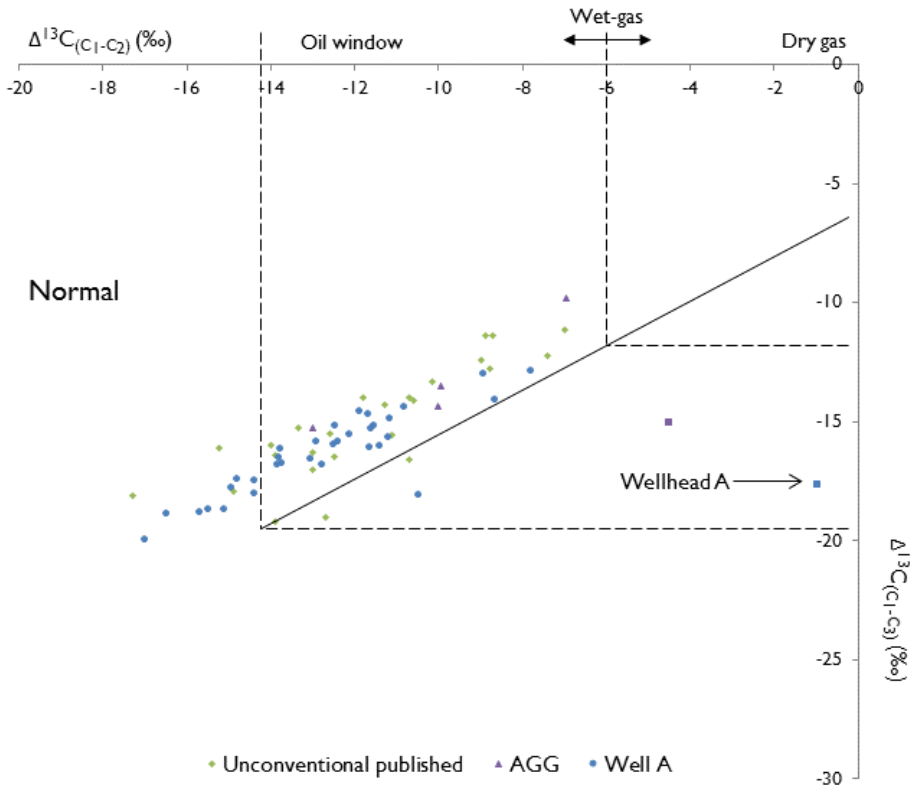

Figure 5. $\Delta^{13}C_{C_1\text{-}C_2}$ versus $\Delta^{13}C_{C_1\text{-}C_3}$ plot of samples from the Montney Formation, including produced gas data already published and other samples measured by the Applied Geochemistry Group (University of Calgary). For the Well A, the samples correspond to mud-gas except the indicated as wellhead.

5. Discussion

5.1 Carbon isotope distribution as an indicator of thermal maturity of natural gas

The strong correlation between the difference of the $\delta^{13}C$ values between methane and ethane and methane and propane for gas samples from different low-permeability reservoirs and their reported thermal maturity based on vitrinite reflectance suggests that $\Delta^{13}C_{C_1\text{-}C_2}$ and $\Delta^{13}C_{C_1\text{-}C_3}$ values can be used as an independent tool to estimate thermal maturity of natural gas from unconventional reservoirs. Based on the currently available data (section 4), we suggest that $\Delta^{13}C_{C_1\text{-}C_2}$ and $\Delta^{13}C_{C_1\text{-}C_3}$ values can be used to assess gas maturity in 5 different categories.

5.1.1 Low maturity interval

$\Delta^{13}C_{C_1\text{-}C_2}$<-15 ‰ and $\Delta^{13}C_{C_1\text{-}C_3}$<-22 ‰ are indicative of immature low-permeability hydrocarbon reservoirs. This low maturity category is represented by gas samples from the Mannville Group (Canada)

which has reported vitrinite reflectance values of 0.3-0.4 % R_o, and the Jafurah Basin (Saudi Arabia) with its maturity being reassessed in section 5.3.1.

5.1.2 Oil window to wet-gas

Gas samples from low-permeability hydrocarbon reservoirs in the oil window and commencement of wet-gas generation are characterized by $\Delta^{13}C_{C_1\text{-}C_2}$ values from -15 to -6 ‰ and by $\Delta^{13}C_{C_1\text{-}C_3}$ values from -20 to -12 ‰ (the 6 and 12 ‰ point being the EID). In the database used for this paper, gas samples from reservoirs in Yanchang (China), Toolebuc (Australia), Baltic and Eastern Pomeranian (Poland), Lorraine, Doig, and Charlie Lake (Canada), Barnett, Clinton/Medina and Woodford (USA) with reported vitrinite reflectance values of 0.8 to 1.5 %R_o fall in this category. The data density for the transition from immature reservoirs to those in the oil window is very sparse, and hence more data from other reservoirs will be required to better define this boundary.

In the oil window and during commencement of wet gas formation, hydrocarbons are generated primarily from kerogen cracking as supported by a relatively constant C_2/C_3 ratio (Prinzhofer and Huc, 1995; see also Figure 3).

5.1.3 Wet-gas to dry gas – normal trend

$\Delta^{13}C_{C_1\text{-}C_2}$ values higher than -6 ‰ and $\Delta^{13}C_{C_1\text{-}C_3}$ values higher than -12 ‰ are accompanied by increasing gas dryness due to wet-gas cracking and can be further sub-divided in three categories based on carbon isotope ratio patterns. The first category represents wet to dry gas with a normal isotope trend ($\delta^{13}C_1 < \delta^{13}C_2 < \delta^{13}C_3$), and is characterized by $\Delta^{13}C_{C_1\text{-}C_2}$ values from -6 ‰ to 0 ‰ and $\Delta^{13}C_{C_1\text{-}C_3}$ values from -12 ‰ to -6 ‰ (i.e. post EID).

This category includes gas samples from hydrocarbon reservoirs such as the Barnett, Clinton/Medina and Woodford (USA), Belcourt, Charlie Lake and Lorraine (Canada), and Western Pomeranian (Poland) with reported vitrinite reflectance data ranging from 1.5 to 2.0 %R_o. While the gas samples in this category are isotopically normal ($\delta^{13}C_1 < \delta^{13}C_2 < \delta^{13}C_3$), an example from the Lorraine Shale, Quebec (Figure 3) indicates that in this region ethane and propane become more depleted in ^{13}C as thermal cracking of wet gas components becomes increasingly important relative to primary cracking of kerogen. Wet-gas cracking is also supported by an increasing C_2/C_3 ratio (Prinzhofer and Huc, 1995; Figure 3). At the same time, this results in increasing gas dryness [measured as $C_1/(C_1+C_2)$] although samples from different reservoirs having the same maturity in the dry gas window will not necessarily have the same gas molecular composition (due to different starting composition at the EID).

5.1.4 Dry gas – ethane isotope reversal

A further increase in reservoir maturity results in gas samples characterized by positive $\Delta^{13}C_{C_1\text{-}C_2}$ values, and hence ethane isotope reversals ($\delta^{13}C_2 < \delta^{13}C_1$), and $\Delta^{13}C_{C_1\text{-}C_3}$ values ranging from -5 to 0 ‰. Samples plotting in this section were derived from Western Pomeranian (Poland), Barnett, Fayetteville and Clinton/Medina (USA), Doig, Belcourt and Charlie Lake (Canada), and Longmaxi (China) with vitrinite reflectance data indicating over-mature samples (>2.0 %R_o). At this stage, thermal cleavage of wet-gas components continues, which results in increasing C_2/C_3 ratios as will be further explained in section 5.2.2.

5.1.5 Dry gas – propane isotope reversal with respect to methane

The highest maturity level for low-permeability hydrocarbon reservoirs in our data set is characterized by gas samples with positive $\Delta^{13}C_{C_1\text{-}C_2}$ and $\Delta^{13}C_{C_1\text{-}C_3}$ values, indicating a propane isotope reversal with respect to methane ($\delta^{13}C_3 < \delta^{13}C_2 < \delta^{13}C_1$ or $\delta^{13}C_{C_2} < \delta^{13}C_{C_3} < \delta^{13}C_{C_1}$). This category is comprised of samples from Fayetteville and Clinton/Medina (USA), Doig, Lorraine, Charlie Lake, Pardonet/Baldonnel, Belcourt and Horn River (Canada), Velkerri (Australia), Longmaxi, Shanxi/Benxi, Wufeng and Black River (China); with reported vitrinite reflectance between 2.5 and 3.3 %. Gas samples from these reservoirs have often very low concentrations of propane and ethane (often close to detection limits) making accurate carbon isotope analyses more challenging.

5.1.6 Relevance of using the carbon isotope distribution as an estimator of thermal maturity

We submit that the here proposed classification of maturity of natural gases from low-permeability hydrocarbon reservoirs, based on carbon isotope data, has several advantages. It provides an independent maturity assessment that is not dependent on rock samples (e.g. vitrinite reflectance) and enables a maturity assessment during drilling of new wells based on the analysis of mud-gas samples provided that adequate sampling is conducted. Furthermore, it allows a refined maturity assessment in the dry gas region with three sub-categories and enables a maturity assessment of gas-condensate accumulations, which overcomes the absence of other thermal maturity molecular indicators such as those based on biomarkers (as biomarkers are often not detected in condensates). Therefore, this approach may be of great value for future maturity assessments of gases from low-permeability reservoirs, especially when other maturity parameters are not available.

Another key aspect is that we are estimating the thermal maturity of the natural gas, which can be equivalent to the thermal maturity of the source rock in case of in-situ generated hydrocarbons. However, some low-permeability reservoirs trapped migrated hydrocarbons before their further burial and maturation. In these cases, the estimation corresponds to the thermal maturity reached in this reservoir and not the maturity of the original source rock. Also, after hydraulic fracturing, natural gas from deeper, more mature reservoir sections may become part of the produced gas stream, which impact the carbon isotope distribution of the produced gas.

We also acknowledge that determination of individual $\%R_o$ values in a depth profile with the corresponding $\delta^{13}C$ of gases may be an avenue for future calculations that increase the certainty of the maturity boundaries.

5.2 Isotope effects controlling the C isotope systematics of C_1-C_3 alkanes

The data evaluated in this manuscript revealed three different regions of C isotope systematics of methane, ethane and propane.

In immature reservoirs, $\delta^{13}C$ values of methane were much more negative than the $\delta^{13}C$ values of ethane ($\Delta^{13}C_{C_1\text{-}C_2}$ <-15 ‰) and $\delta^{13}C$ values of propane were 3 to 7 ‰ higher than those of ethane (Figures 2e-h). This normal and uneven C isotope distribution resembles the distribution frequently reported for natural gas occurrences in conventional reservoirs (e.g. Berner et al., 1995; Rooney et al., 1995; Berner

and Faber, 1996; Whiticar, 1999; Milkov and Etiope, 2018) and is predominantly controlled by kinetic isotope effects. Carbon isotope equilibrium is not expected at low maturity due to the slow kinetics of the system (e.g. Sherwood Lollar et al., 2008; Thiagarajan et al., 2020). It may seem surprising to find thermogenic gas in very immature source rocks such as the Mannville Group (0.4 $\%R_o$) and some biogenic gas contributions cannot be ruled out. Our data set contains very few data for gases from low maturity reservoirs (probably due to low production). Therefore, this section of Figure 4 requires further investigations and refinement in a future study.

In reservoirs where the source rock reaches the oil window, we observed a different pattern, where the distribution of $\delta^{13}C$ values is still normal ($\delta^{13}C_{C_1} < \delta^{13}C_{C_2} < \delta^{13}C_{C_3}$) but the difference of $\delta^{13}C$ of methane and ethane and ethane and propane approaches a similar value near -6 ‰ (Figures 2e-h) at a thermal maturity of 1.5 $\%R_o$. We propose that this even isotopic distribution (EID) of C_1-C_3 alkanes in the oil window is possibly controlled by thermodynamic/equilibrium isotope effects, revealing an increased tendency towards isotope exchange reactions taking place under these conditions. This process is typically favored in systems where the phases (e.g. C_1-C_3 alkanes) have remained in close proximity over an extended period of time (Kaye, 1992; Chacko et al., 2001), a condition favored in many low-permeability reservoirs.

This notion is supported by the observation that the C isotope distribution pattern at 1.5 $\%R_o$ differs from the models commonly applied for the genetic characterization of natural gas. To illustrate this we plotted the $\Delta^{13}C_{C_1\text{-}C_2}$ and $\Delta^{13}C_{C_1\text{-}C_3}$ values of the two Rayleigh fractionation models by Clayton (1991a and b, Figure 6a), the isotope exchange model by James (1983; Figure 6a), and the pattern observed in this study in Figure 6b, all at the same thermal maturity of 1.5 $\%R_o$. We suggest that in low-permeability hydrocarbon reservoirs in the oil window, where C_1-C_3 alkanes have remained in close proximity over an extended period of time, a tendency towards attaining isotope equilibrium partially controls the $\delta^{13}C$ values of C_1-C_3 alkanes and may result in EID. The main difference with James' model (1983) is that this author assumed equilibrium isotope effects to commence at lower thermal maturity than the oil window. In our view, this is questionable because kinetic isotope effects are potentially more prominent at early stages due to lower temperatures and lower generation rates (Lorant et al., 1998; Sherwood Lollar et al., 2008; Mango et al., 2009).

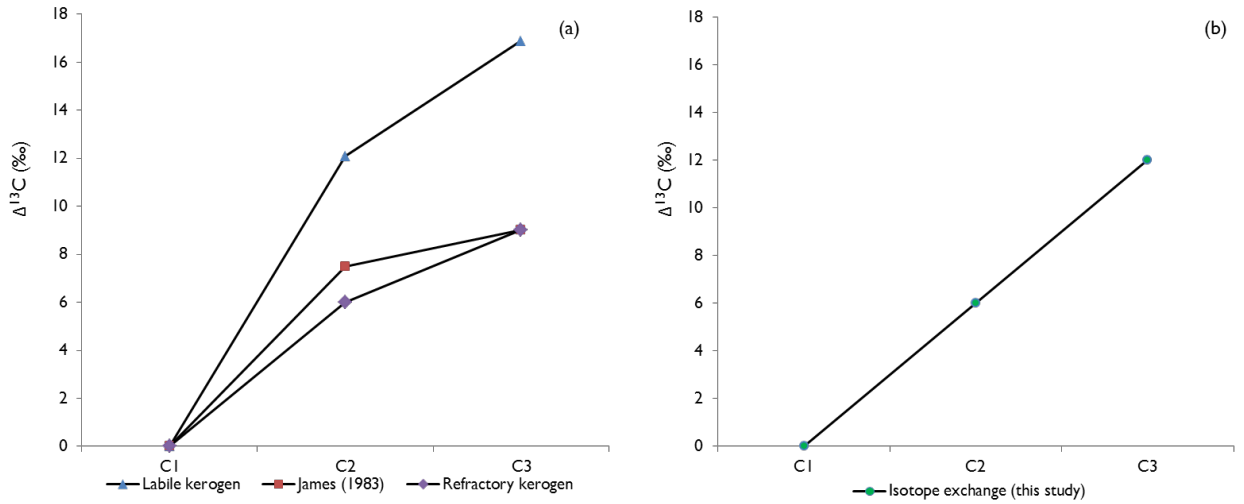

Figure 6. Different isotopic fractionation models for (a) C_1-C_3 alkanes from natural gas at 1.5 $\%R_o$ including the Rayleigh model for labile kerogen and refractory kerogen (Clayton 1991a) and the isotope exchange model by James (1983), and (b) the EID from this study.

More recently, Abrams (2017) adapted the principles of James (1983; 1990) to construct a classification plot based on the C isotope ratio of methane plotted versus the difference of the carbon isotope ratios of ethane and propane. Figure 7 shows this classification and reveals that a large portion of our data set for samples from low-permeability reservoirs plots outside of the boxes indicated by Abrams (2017). Although Abrams (2017) acknowledged potential variations in $\delta^{13}C$ of methane (x axis) due to organic facies, we observed that most of the deviations of our data from the model shown in Figure 7 are due to elevated $\delta^{13}C_{C_2} - \delta^{13}C_{C_3}$ values (y-axis). The observed deviations occur predominantly in samples with isotope reversal, an effect that was not taken into account. It is also noteworthy that Figure 7 plots the difference between the $\delta^{13}C$ of ethane and propane in absolute values, which results in gases from very different maturity in our dataset (less mature $\delta^{13}C_{C_2} < \delta^{13}C_{C_3}$ and highly mature $\delta^{13}C_{C_3} < \delta^{13}C_{C_2}$) plotting together.

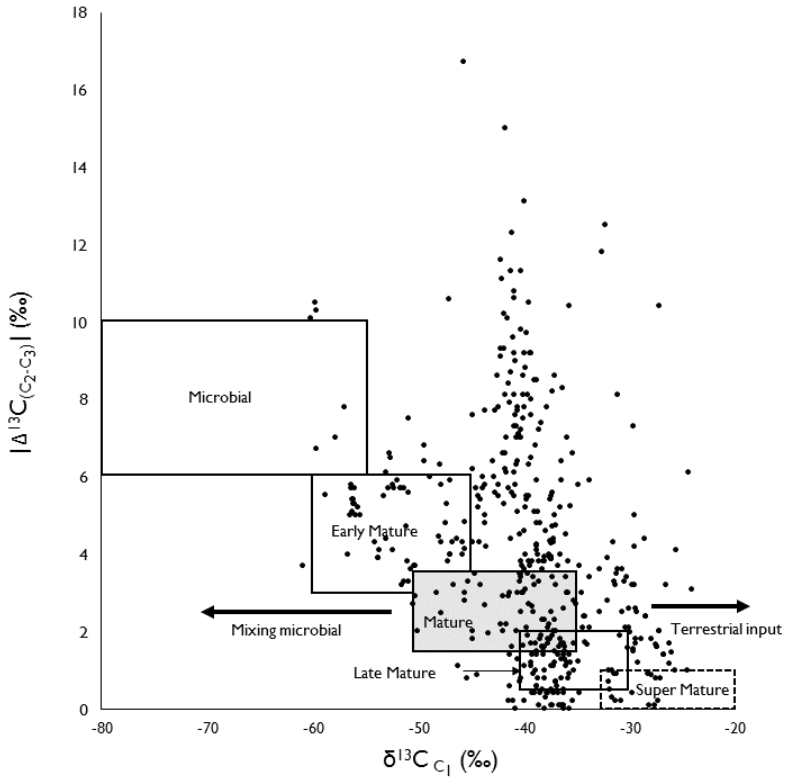

Figure 7. Gas samples from low-permeability reservoirs (this study) represented in a compound specific carbon isotopic analysis interpretation chart by Abrams (2017) after James (1983, 1990).

Further increasing maturity of low-permeability hydrocarbon reservoirs results in dry gas conditions, where $\Delta^{13}C_{C_1\text{-}C_2}$ and $\Delta^{13}C_{C_2\text{-}C_3}$ values continue to increase at a similar rate (Figures 2e-h) and methane, ethane and propane maintain similar $\Delta^{13}C$ values between them. As thermal maturity further increases, C isotope systematics progress first towards ethane isotope reversals ($\delta^{13}C_{C_2} < \delta^{13}C_{C_1} < \delta^{13}C_{C_3}$), and subsequently to propane isotope reversal with respect to methane where $\delta^{13}C_{C_3} < \delta^{13}C_{C_2} < \delta^{13}C_{C_1}$ or $\delta^{13}C_{C_2} < \delta^{13}C_{C_3} < \delta^{13}C_{C_1}$ (Figure 4). This indicates that thermodynamic/equilibrium isotope effects no longer provide the predominant control on the $\delta^{13}C$ values of C_1-C_3 alkanes, but that additional processes affect the C isotope distribution of methane, ethane and propane under these highly mature conditions.

Below, we further elaborate on the processes governing the normal even-isotopic-distribution (EID) of -6 ‰ and isotope reversal conditions that appear to be unique for low-permeability hydrocarbon reservoirs that have reached the oil and dry gas windows.

5.2.1 Isotope exchange and chemical equilibrium

Even though isotope exchange can take place in chemically equilibrated systems as well as in systems that are not at chemical equilibrium (Cole and Chakraborty, 2000), we have tested whether the molecular composition of natural gas from low-permeability reservoirs is under equilibrium constraints. For this purpose we use data from the Barnett Shale as this low-permeability hydrocarbon reservoir covers the entire oil window, which is the interval where isotope exchange is postulated to be the predominant

process. We have calculated the same chemical parameters (see Table S4) for the other shale plays to validate that our observations are generally applicable.

The chemical equilibrium of C_1-C_3 in natural gas has been suggested to occur through gas metathesis, and is only possible through mineral catalysis (Mango et al., 2009, Mango and Jarvie, 2009, 2010). The process consists of molecular inter-conversion as a molecule C_n splits to smaller intermediates (e.g. radicals) on a single metal site, and these bond to other radicals to form new molecules (Mango et al., 2009; Mango and Jarvie, 2010). Gas metathesis of C_1-C_3 is defined by equation 1, and its equilibrium constant K corresponds to equation 2 (Mango et al., 2009).

$$2C_2H_6 \leftrightarrows CH_4 + C_3H_8 \qquad \text{(equation 1)}$$

$$K = [(CH_4).(C_3H_8)]/[(C_2H_6)^2] \qquad \text{(equation 2)}$$

Figure 8 shows molecular data for samples from the Barnett Shale on a modified equilibrium plot (after Mango et al., 2009). The strong correlation between the factors $(C_2H_6)^2$ and $(CH_4).(C_3H_8)$ suggests a gas composition near equilibrium, with a Q quotient approximately constant at 2.5 (see also Table S4), identical to the Q value found for the Barnett Shale by Mango et al. (2009). The reaction quotient Q is calculated as K (equation 2) but it is termed Q when it is unknown whether the system has reached chemical equilibrium, and it is commonly accepted that a constant Q suggests proximity to equilibrium (Q~K, e.g. Duffey, 2013). Additionally, the thermal maturity assignments of the samples belonging to the oil window and the dry-gas window based on the $\Delta^{13}C_{C_1\text{-}C_2}$ and $\Delta^{13}C_{C_1\text{-}C_3}$ plot (Figure 4) confirm that the equilibrium factors $(C_2H_6)^2$ and $(CH_4).(C_3H_8)$ decrease with increasing gas dryness as suggested by Mango et al. (2009). Nonetheless, the Q quotient of the Barnett Shale does not fall within the equilibrium limits calculated by Mango et al. (2009) using thermodynamic data, which are Q = 25.12 at 52 °C and Q = 5.37 at 300 °C.

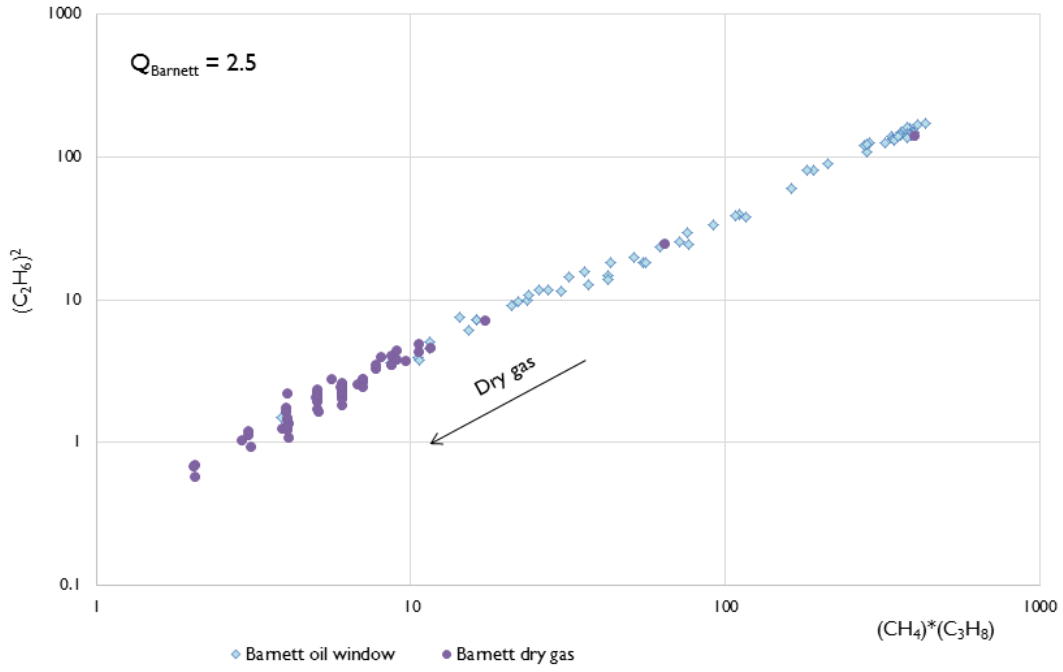

Figure 8. Equilibrium plot (modified after Mango et al., 2009) for samples from the Barnett Shale. The distinction of wet-gas samples versus dry-gas samples is based on Figure 4 and the EID. $Q = [(CH_4).(C_3H_8)]/[(C_2H_6)^2]$, using the vol % composition of the C_1-C_5 compounds in natural gas.

If metathesis requires mineral catalysis, the catalytic effect will vary from one reservoir rock type to another and thus not all systems would reach chemical equilibrium at the same time and temperature. In fact, a metathetic reaction under equilibrium control can still yield hydrocarbons out of equilibrium concentrations (Mango et al., 2009). Therefore, different Q quotients are expected for different reservoir rocks (Table S4) when equilibrium is not attained, or even if equilibrium is attained but reservoir temperatures vary (as the equilibrium constant depends on temperature). For example, Q varies from 4.9 to 9.3 in gas samples from Black River, from 2.5 to 6.8 in Clinton/Medina, from 2.0 to 7.0 in the Woodford Shale, and from 1.5 to 7.5 in the Lorraine Shale (the latter having increased compositional variability as samples were collected in IsoJars). Non-equilibrated gases from low permeability reservoirs could also be a consequence of primary production of disequilibrium methane, ethane and propane through kerogen cracking occuring much faster than metathesis. This requires further investigation and would also be associated to the gas residence time in the reservoir for chemical equilibrium to be attained.

As Lorant et al. (1998), Mango et al. (2009) also highlighted the importance of residence time of the gas because they noticed during closed system pyrolysis experiments that gases from the New Albany Shale (initially removed from equilibrium) tended towards equilibrium with increasing residence time and gas dryness. Another key element favoring metathesis, and thus equilibrium, may be the phase states of hydrocarbons. For example, in conventional petroleum systems hydrocarbons accumulate as free oil and gas, whereas in low-permeability reservoirs the oil occurs in free state, but the majority of the gas may be stored as absorbed/adsorbed or dissolved gas (Zhao et al., 2019), which may facilitate mineral catalyzed transformations.

We conclude that, although the molecular composition of the hydrocarbon charge can be under equilibrium constraints, the carbon isotope trends that we have observed in this study, including the even isotope distribution (EID), occur independent of whether chemical equilibrium is achieved.

5.2.2 The isotope equilibrium

It is important to emphasize that the EID is an empirical observation from the database collected for this study. The EID does not represent carbon isotope fractionation factors. Further modelling is required to perform an isotope balance that can explain EID in different natural gases independently from the starting $\delta^{13}C$ value of the parental kerogen.

Carbon isotope equilibrium exchange among methane, ethane and propane molecules may occur through elemental chemical reactions or intermolecular collision (Chacko et al., 2001). However, the mineral-catalyzed gas metathesis suggested by Mango et al. (2009) also seems to be a viable mechanism for isotope exchange due to the molecular inter-conversion between methane, ethane and propane.

In isotope equilibrium the isotopic difference between compounds depends only on temperature and not on the relative distribution of material (or molecular distribution) between them (Hayes, 1993). Lorant (1998) found that the source of gas (as a determining factor for the molecular composition) has a limited effect on the isotopic composition of alkane gases in a closed-system, and suggested that the key factors

controlling the isotopic composition of gases in closed systems are the temperature and the residence time of the gas in the source rock. The second factor does not play a major role in conventional petroleum systems because these behave as open systems in which natural gases generally have low residence times in the source rock with respect to their generation rate (Lorant, 1998). In Figure 9a we have plotted the difference between $\delta^{13}C$ values of ethane and propane versus the C_2/C_3 ratio similar to the diagram of Prinzhofer and Huc (1995) modified after Lorant (1998), and compare gases from open systems, the closed system trend observed by Lorant (1998), and gases from the Lorraine Shale reservoirs (a semi-closed system) which range from the oil window to dry-gas window (see also section 2). This type of diagram removes interference due to methane migration (Prinzhofer and Huc, 1995), and confirms the trend in $\delta^{13}C$ values of ethane and propane towards a constant difference of ≈6 ‰ (the EID) after the oil window, with only minor variations of the C_2/C_3 ratio (as described in section 4.2). A relatively constant C_2/C_3 ratio is indicative of hydrocarbons resulting from primary cracking of kerogen, as also mentioned in section 5.1.2 (Prinzhofer and Huc, 1995). After the EID value of 6 ‰ is reached, the C_2/C_3 ratio increases while the $\Delta^{13}C_{C_2\text{-}C_3}$ value becomes initially more negative and subsequently increases to higher values trending towards zero (Figure 9a; see also Figure 2 and 3). The increasing C_2/C_3 ratio suggests thermal cracking of wet gas components preferentially producing ethane over propane with increasing maturity (Prinzhofer and Huc, 1995; see also Figure 3e,f, and sections 4.2 and 5.1.3). The change in the $\Delta^{13}C_{C_2\text{-}C_3}$ value occurs because the $\delta^{13}C$ values of ethane and propane start to decrease at these conditions, as described in section 4.2.

Similar trends are observed in other reservoirs such as the Barnett Shale (Figure 9b) and the Pomeranian Basin (Figure 9c), but the initial C_2/C_3 ratio and the magnitude of its increase varies. For example, the initial C_2/C_3 ratio is around 1.0 for the Lorraine shale, 2.6 for the Barnett shale, and 2.0 for Pomeranian (Figure 9). Such variability does not affect the trend towards an even isotopic distribution of ≈ 6 ‰ where a tendency towards attaining isotope equilibrium was observed.

Pressure may be another parameter to affect isotope equilibrium in a low-permeability reservoir, but we found no evidence for this. The fact that we were able to compare reservoirs with different porosities and permeability suggests that pressure does not play a major role in the isotope exchange. In fact, pressure effects on equilibrium isotope exchange have only been found at higher pressure and temperature windows, e.g. in the graphite-diamond system (Polyakov and Kharlashina, 1994). Hence we conclude that the carbon isotope distribution of C_1-C_3 alkanes in the oil-window of low-permeability hydrocarbon reservoirs that display a tendency towards attaining isotope equilibrium depends solely on temperature.

Recently, some gases in isotope equilibrium were reported by Thiagarajan et al. (2020) (gases from the USA, Germany, and Norway). Their observations were consistent with a metastable cyclic equilibrium, also supported by clumped-isotopes measurements. Their study is rather fundamental and does not allow gas classification nor explains the isotope reversal phenomenon, but it does support kinetic isotopic fractionation (non-equilibrium) at low thermal maturity and tendency to thermodynamic equilibrium with increasing temperatures.

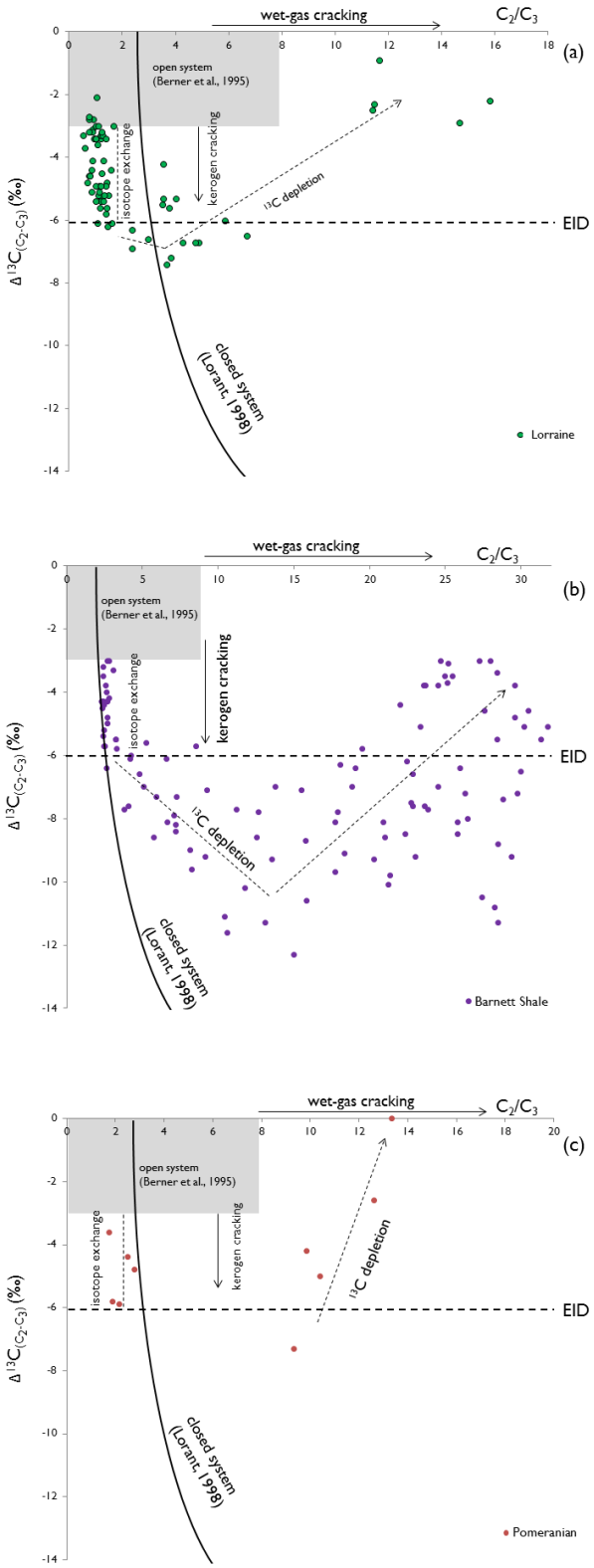

632

633 **Figure 9**. Prinzhofer and Huc diagram, modified after Lorant (1998) for (a) the Barnett Shale, USA (b) Pomeranian,
634 Poland, and (c) Fortierville/Leclercville, Lorraine Shale, Canada.

5.2.3 The isotope reversal phenomenon

As thermal maturity further increases, C isotope systematics progress first towards ethane isotope reversal ($\delta^{13}C_{C_2} < \delta^{13}C_{C_1} < \delta^{13}C_{C_3}$), and subsequently to propane isotope reversal with respect to methane where $\delta^{13}C_{C_3} < \delta^{13}C_{C_2} < \delta^{13}C_{C_1}$ or $\delta^{13}C_{C_2} < \delta^{13}C_{C_3} < \delta^{13}C_{C_1}$ (Figure 4). In Figure 3 we had observed that at the EID the *i*C_4/*n*C_4 ratio starts to decrease due to thermal cracking of wet-gas compounds (section 4.2). At the same depth, $\delta^{13}C$ values of ethane and propane start to progressively decrease with increasing depth (Figures 3i-l), which is highly unusual in conventional reservoirs. The co-occurrence of these trends provides very strong evidence that additional processes are occurring in the dry gas window resulting in an enrichment of ^{12}C in ethane and in propane. The decreasing $\delta^{13}C$ values for ethane and propane progressively result in the observed phenomenon of ethane isotope reversal and subsequent propane isotope reversal with respect to methane (Figure 4) as maturity increase towards highest levels.

It is unknown to what extent carbon isotope exchange continues after EID is initially reached. The linearity of the data in the $\Delta^{13}C_{C_1\text{-}C_2}$ versus $\Delta^{13}C_{C_1\text{-}C_3}$ plot (Figure 4) weakens somewhat, which suggests that the processes controlling the isotopic distribution are not the same as those earlier in thermal history. It is possible that thermal cracking of wet-gas components (e.g. pentanes and butanes) in the gas window results in an enrichment of ^{12}C in ethane and propane, as it was described by Xia et al (2012) and also adopted by Tilley and Muehlenbachs (2013). However, it is also possible that ethane and propane decompose, and normal kinetic carbon isotope effects during thermal decomposition result in ^{13}C enrichment of residual ethane and propane (Tang et al. 2000; Xia and Gao, 2018) which would not explain the trends in our dataset. In fact, the mixing of gas from kerogen cracking with gas oil/wet-gas cracking has been found to not satisfy the mass and isotope balance during isotope reversal (Xia and Gao, 2018).

The formation of ^{13}C depleted ethane and propane is likely caused by high temperature reactions that can involve geopolimerization of methane (Zeng et al., 2013) or regeneration of ethane via reversible free radical reactions catalyzed by minerals (Xia and Gao, 2018). Xia and Gao (2018) found that during thermal decomposition of ethane and propane at high maturity partly reversible free radical reactions were necessary to satisfy the C_1-C_3 mass and isotope balance, and the isotope reversal would depend on the rate and kinetic isotope effects of these reactions. The same authors emphasize that free radical concentration vary in different geological settings, thus this set of reactions will not proceed in the same way in all source rocks. This may explain the data dispersion in the propane reversal section of Figure 4. The possibility of reversible free radical reactions does not necessarily imply that the abundance of ethane and propane will increase at high maturity (Xia and Gao, 2018).

Note that these mineral-catalyzed transformations are different from metathesis. Metathesis implies a displacement/interconversion reaction that favors isotope exchange whereas the regeneration of ethane and propane resulting in ^{12}C enrichment in ethane and propane and hence isotope reversal is a protonation+polymerization reaction (Xia and Gao, 2018). Natural gases of potentially abiogenic origin with ethane isotope reversals have also been proposed to form via kinetically controlled polymerization reactions (Sherwood Lollar et al., 2002, 2006, 2008).

From the molecular point of view, Figure 10 shows that the equilibrium factors $(C_2H_6)^2$ and $(CH_4).(C_3H_8)$ remain constant after the EID is reached at $\Delta^{13}C_{C_1\text{-}C_2}$ of 6 ‰. This does not only imply that reverse

674 reactions to form ethane and propane may be occurring, but also that the formation of ^{13}C depleted
675 ethane and propane could be a consequence of the system trying to sustain chemical and isotopic
676 equilibrium. The factors controlling which of the three reactions (metathesis, free radical
677 decomposition/polymerization, and thermal cracking) is predominant in a particular reservoir may be an
678 interesting avenue of future research. The observed trends indicate that thermodynamic/equilibrium
679 carbon isotope effects no longer provide the sole control on the $\delta^{13}C$ values of C_1-C_3 alkanes in the dry
680 gas window.

681

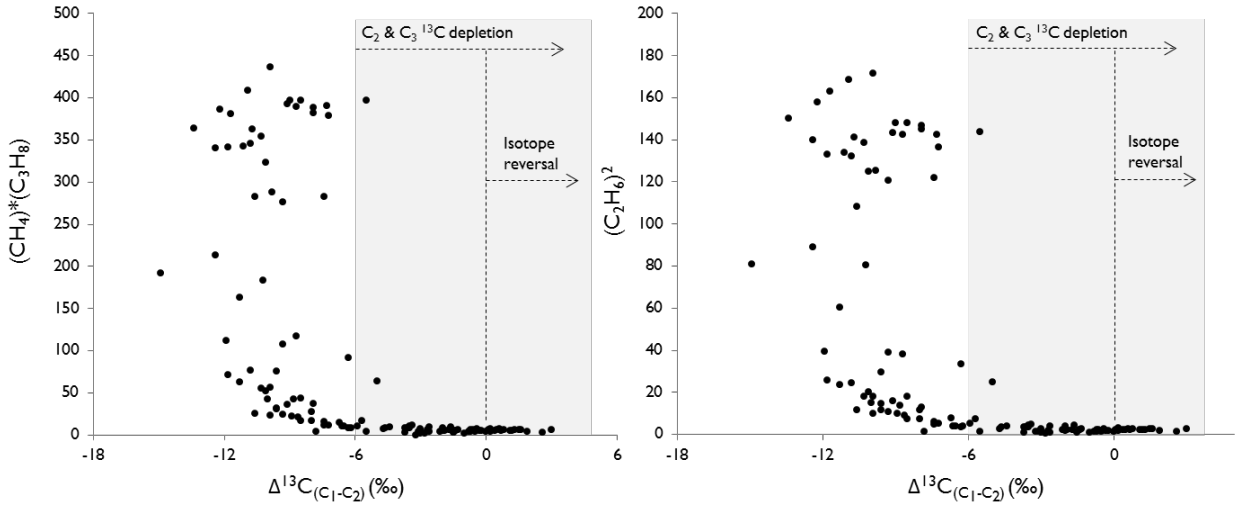

682

683 **Figure 10**. Gas metathesis equilibrium factors $(CH_4).(C_3H_8)$ and $(C_2H_6)^2$ versus of the $\Delta^{13}C_{C_1\text{-}C_2}$ of Barnett Shale.

684 A ^{13}C depletion may not be observed in methane after the EID because it has been found that during
685 thermal cracking of oil/wet-gas most of the methane continues to be formed from residual kerogen
686 cracking (highly ^{13}C enriched methane), while thermal cracking of larger oil/wet-gas components
687 preferentially produces ethane and propane (e.g. Prinzhofer and Huc, 1995; Xia et al., 2012; Liu et al.,
688 2019).

689 It is also important to note that some low-permeability reservoirs may contain hydrocarbons that migrated
690 some distances from the original source rock and have not equilibrated in the reservoir due to short
691 residence times. Some of these migrated hydrocarbons might have not experienced significant thermal
692 degradation after entrapment. These gases may not follow the trends observed in this study as their
693 aforementioned factors (migration and residence time) would have broken and/or delayed the equilibrium.

694 *5.3 Practical applications*

695 The described trends of the $\Delta^{13}C_{C_1\text{-}C_2}$ and $\Delta^{13}C_{C_1\text{-}C_3}$ values and the relationship of these parameters with
696 reservoir maturity have a number of practical applications, with three examples provided below.

697 *5.3.1 Reassessing thermal maturity – Jafurah Basin, Saudi Arabia*

Figure 4 plots the samples from the Jarufah Basin (Table S3), Saudi Arabia, derived from Hakami et al. (2016) in the low maturity region of the $\Delta^{13}C_{C_1\text{-}C_2}$ versus $\Delta^{13}C_{C_1\text{-}C_3}$ diagram. This assessment indicates a lower thermal maturity than suggested by Hakami et al. (2016) for these rocks, who reported a thermal maturity of >1 $\%R_o$ of estimated vitrinite reflectance equivalent (VRE) using the conversion by Jacob (1989) based on Tmax and solid bitumen reflectance. The same authors also noted that Tmax values derived via rock-eval were lower in kerogen isolates compared to whole-rock analyses.

In a second study using different conversion formulas, Hakami and Inan (2016) found thermal maturity for the Tuwaiq Formation (the deepest rock with hydrocarbon potential) of 0.62 % VRE. It has been demonstrated that the presence of solid bitumen leads to erroneous rock-eval analysis results (Chatellier et al., 2013; Wood et al., 2018) and therefore it is not surprising that the estimations of thermal maturity using bitumen reflectance in these rocks can be largely variable. Additionally, $\delta^{13}C$ values for methane as low as -60 ‰, as found in the Jarufah Basin (Table S3), are not very common within the oil window (e.g. Whiticar, 1990; 1994; Milkov and Etiope, 2018). The use of the $\Delta^{13}C_{C_1\text{-}C_2}$ versus $\Delta^{13}C_{C_1\text{-}C_3}$ diagram provides an alternate avenue to assess the thermal maturity of this reservoir potentially in a more accurate fashion, and suggests a thermal maturity of 0.4 to 0.8 $\%R_o$ for the Jafurah Basin samples.

5.3.2 Isotopic characterization of the Montney Formation, WCSB

The complexity of the Montney Formation is based on the fact that it is a hybrid system where fluid migration has occurred to some extent and there are no clear limits between open and semi-closed sections (e.g. Kuppe et al., 2012; Tilley and Muehlenbachs, 2013). However, it is known that migrated hydrocarbons were trapped in the Montney Formation before its further burial and thermal maturation (circa 60 Ma; Ness, 2001). Significant gas migration has occurred after the Eocene due to uplifting (Wood and Sanei, 2016), particularly in the Alberta section. The residence time of the gas formed in low-permeability portions of the reservoir prior to its migration to other reservoir sections within the same play remains unclear.

Data for mud-gas samples shown in Figure 5 reveal that the Montney Formation is in the oil window consistent with findings from previous research (e.g. Riediger, 1997; Rokosh et al., 2012). However, the produced gas (well A) is very close to ethane-reversal. We suggest that the produced gas from well A represents a mixture of more mature ethane-reversed gas with less mature gas in normal isotope trend (as classified in Figure 4). A more mature gas input was probably accessed as a consequence of hydraulic fracturing. Chatellier and Perez (2015) detected gases in ethane isotope reversal in some areas of the Montney Formation although none of these data are publically available. We continue to study the Montney Formation and other reservoirs in the WCSB, and aim to develop new geochemical tools that can explain fluid distributions in these reservoir rocks, particularly light hydrocarbons, which display considerable variability in different locations in the same play.

5.3.3 Thermal maturity indicated by gas samples from the Southern Anadarko Basin Oklahoma (SCOOP) play

Recently, Abrams and Thomas (2020) analyzed produced gas and oil from the Woodford Shale in the SCOOP play. The authors could not explain the discrepancy between thermal maturity estimations based on oil versus gas analyses. The authors used the heptane value to estimate a maturity between 0.85 and 1.5 $\%R_o$ for liquid hydrocarbons. However, when estimating thermal maturity based on gas isotopes using

James' approach (1983, 1990), the results indicated 0.5 to 0.7 $\%R_o$. They were not able to find an explanation for the gas being less mature.

In Figure 11 we have plotted the carbon isotope data for samples reported in Abrams and Thomas (2020) (see also Table S5) using the thermal maturity tool proposed in this study. Our estimation suggests a thermal maturity of the natural gas between 0.8 and 1.5 $\%R_o$ which perfectly matches the thermal maturity indicated by the oils. This suggests that James' isotope model (1983, 1990) may not be suitable to interpret the geochemistry of these gas samples from the Woodford Shale. The finding also supports the source independence of our gas maturity assessment tool. For example, gases with very different individual $\delta^{13}C$ values (affected by source) can correspond to a similar thermal evolution as it is the case of some gases from the Montney Formation (e.g. $\delta^{13}C_{C_1}$ -42‰, $\delta^{13}C_{C_2}$ -28‰, $\delta^{13}C_{C_3}$ -23‰) and the Woodford Shale (e.g. $\delta^{13}C_{C_1}$ -53‰, $\delta^{13}C_{C_2}$ -39‰, $\delta^{13}C_{C_3}$ -34‰).

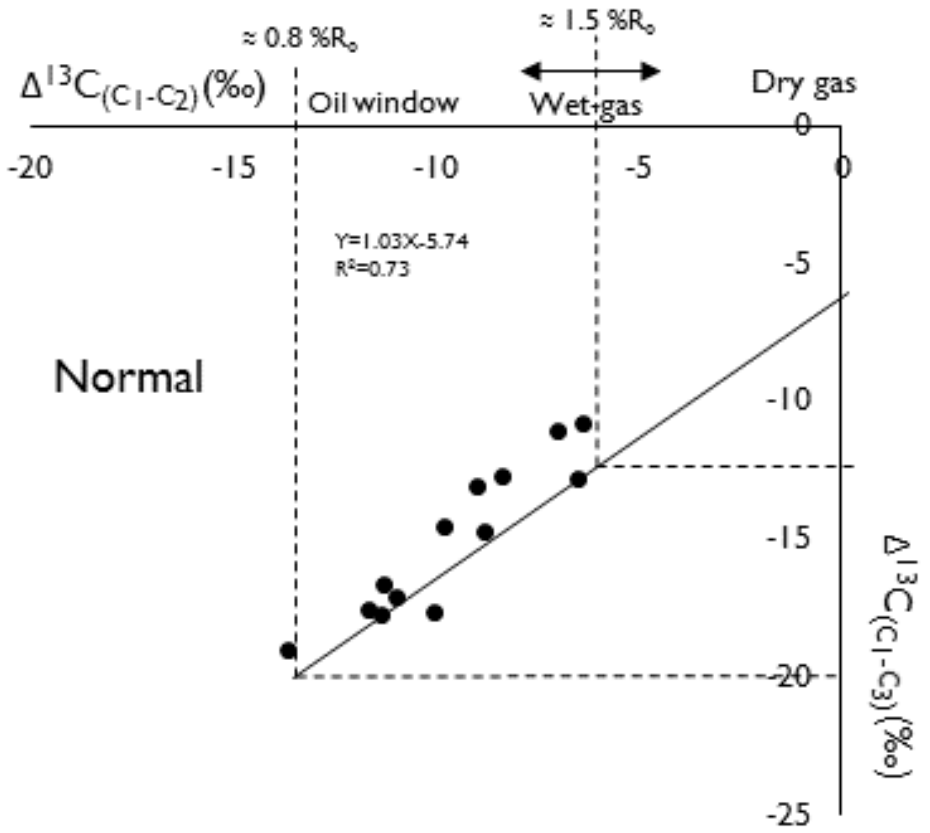

Figure 11. The $\Delta^{13}C_{C_1\text{-}C_2}$ versus $\Delta^{13}C_{C_1\text{-}C_3}$ plot for gas classification. Gas samples from the Woodford Shale in the SCOOP play. Data from Abrams and Thomas (2020).

5.4 Mud-gas versus produced gas

The majority of data points collected in this study correspond to produced gas (see also Table S3). Mud-gas data were only presented for the Lorraine Shale from Quebec as this is the most comprehensive profile available for gases generated in-situ from a single shale in a key range of maturity (oil window to dry gas) found in the literature. More importantly, these samples were collected in IsoJars (gas desorbed from cutting samples) at least 25 m apart which decreases the uncertainty of samples depth and the possibility of free gas mixing. We also used mud-gas samples collected in IsoTubes from the Montney Formation while ensuring that all these samples were derived from only the Montney Fm. and a distinction between Montney intervals was not attempted. Mud-gas samples were also presented for the low-maturity region of Figure 4 as they were the only data available in the literature for such a low maturity interval (probably because gas production is insufficient for economic recovery). We acknowledge that differences between MGIL data (mud-gas isotope logging) and produced gas data can occur. For instance, the mud-gas samples in IsoTubes represent the free gas released during drilling through a given reservoir section, whereas the produced gas is the total gas combination that flows after hydraulic fracturing. The hydraulic fracturing process generates access to new sections of the reservoir where fluids with a higher maturity signature could have been accumulated and are now accessed (Tilley and Muehlenbachs, 2013; Zhang M. et al., 2018).

Temporal changes may occur in the chemical and isotopic composition of produced gas. In a 3.5 years experiment, Zhang M. et al. (2018) found very minor fluctuations in the isotopic composition of produced gas from the Longmaxi Formation, China. The authors indicated that this was due to an adequate gas supply from the matrix to the fracture network, and the homogeneity of lithofacies in this reservoir. In contrast, Norville (2014) reported disparity between mud-gas and produced gas C isotope ratios, as well as ubiquitous temporary variations in $\delta^{13}C$ of C_1-C_3 in the Muskwa Otter Park Formations (Horn River Basin, Canada), and attributed such variability to a heterogeneous lithology (mineralogy, shale fabric and flow connectivity). These considerations must also be taken into account when interpreting gas isotope data for samples from low-permeability hydrocarbon reservoirs using the tools proposed here.

6. Conclusions

We conclude that isotopic models and tools (e.g. diagrams and mathematical regressions) for interpreting the $\delta^{13}C$ values of C_1-C_3 alkanes in low-permeability hydrocarbon reservoirs are in part different to those that were designed for conventional hydrocarbon accumulations that resemble an open system with low residence times of hydrocarbons in the source rock. Low-permeability reservoirs are semi-closed systems that generate and/or accumulate hydrocarbons over long residence times. These conditions lead to a distribution of stable carbon isotope ratios of *n*-alkane gases that differs from isotope models previously conceived for conventional hydrocarbon reservoirs.

The presented data suggest that the stable carbon isotope distribution of natural gas from low-permeability reservoirs cannot be explained by Rayleigh distillation nor by James' isotope equilibrium model. The $\delta^{13}C$ values of C_1-C_3 alkanes in low-permeability reservoirs initially increase with increasing thermal maturity. During the oil/wet-gas window, the $\delta^{13}C$ of methane, ethane and propane reach an even carbon isotopic difference of approximately 6 ‰ between compounds (EID) at 1.5 $\%R_o$, before wet-gas cracking becomes increasingly important. We suggest that the EID isotopic distribution is a consequence of an increased tendency towards isotope exchange reactions (potentially via metathesis). This indicates that carbon

isotopic fractionation influencing $\delta^{13}C$ values of C_1-C_3 alkanes is additionally affected by partial isotopic equilibration from the start of the oil window until 1.5 $\%R_o$.

At higher thermal maturity in the dry gas window, isotope exchange occurs simultaneously with thermal cleavage of wet-gas components and potentially abiogenic polymerization of alkane gases and other free radical reactions (occurring under normal kinetic isotope effects) to sustain the system in isotopic equilibrium. Thermal cleavage of wet-gas components and abiogenic polymerization of alkane gases are probably the main mechanism generating ^{13}C depleted ethane and propane. The newly formed ethane and propane with low $\delta^{13}C$ values results in the frequently observed isotope-reversal ($\delta^{13}C_{C_2} < \delta^{13}C_{C_1} < \delta^{13}C_{C_3}$, $\delta^{13}C_{C_2} < \delta^{13}C_{C_3} < \delta^{13}C_{C_1}$, and $\delta^{13}C_{C_3} < \delta^{13}C_{C_2} < \delta^{13}C_{C_1}$) characteristic for high maturity low-permeability hydrocarbon reservoirs.

The $\Delta^{13}C_{C_1\text{-}C_2}$ versus $\Delta^{13}C_{C_1\text{-}C_3}$ plot proposed in this study represents a practical tool for classification of natural gas from low-permeability hydrocarbon reservoirs, and separates the samples according to thermal history, in three regions: normal trend (subdivided into immature, oil/wet-gas window, and dry gas window), ethane reversal, and propane reversal with respect to methane. This classification is valid for the data presented in this paper but might vary according to the openness of the system and the residence time of hydrocarbons in the source rock.

Given the somewhat unclear boundaries between closed, semi-closed and open systems in the geological context, and the fact that gas generation is a dynamic process, we recommend that it is advisable to refer to the degree of openness of the system in dependence of the residence time of gas hydrocarbons in the reservoir where they formed. A longer residence time in low-permeability reservoirs, for a given thermal history and generation rate, is most likely responsible for the unique carbon isotope distributions found in natural gases obtained from low-permeability hydrocarbon reservoirs independent on the sampling approach.

Acknowledgements

This research was undertaken thanks in part to funding from the Canada First Research Excellence Fund. J.C. acknowledges MITACS and KERUI Petroleum for supporting the postdoctoral position. The authors also acknowledge ARC Resources Ltd. for providing samples. The authors highly appreciate the feedback and suggestions from Dr. Michael A. Abrams and an anonymous reviewer to improve the quality of this article.

Declaration of Interest

The authors declare no competing interest.

Data availability

The data presented in this study can be found in the supplementary material.

References

828 Abrams M. A. (2017) Evaluation of near-surface gases in marine sediments to assess subsurface petroleum
829 gas generation and entrapment. *Special Issue of Geosci. J.: Natural Gas Origin, Migration, Alteration and Seepage*
830 **7**, 35.

831 Abrams M. A. and Thomas D. (2020) Geochemical evaluation of oil and gas samples from the Upper
832 Devonian and Mississippian reservoirs Southern Anadarko Basin Oklahoma and its implication for the
833 Woodford Shale unconventional play. *Mar. Petrol. Geol.* **112**, 1-17.

834 BC Oil and Gas Commission (2012) *Montney Formation Play Atlas NEBC*. Government of British Columbia,
835 Canada, pp. 36.

836 Berner U. and Faber E. (1988) Maturity related mixing model for methane, ethane and propane, based on
837 carbon isotopes. *Adv. Org. Geochem.* **13** (1-3), 67-72.

838 Berner U., Faber E., Scheeder G. and Panten D. (1995) Primary cracking of algal and land plant kerogens:
839 kinetic models of isotope variations in methane, ethane and propane. *Chem. Geol.* **126**, 233-245.

840 Berner U. and Faber E. (1996) Empirical carbon isotope/maturity relationships for gases from algal
841 kerogens and terrigenous organic matter, based on dry, open-system pyrolysis. *Org. Geochem.* **24**, 947-
842 955.

843 Burrus R.C. and Laughrey C.D. (2010) Carbon and hydrogen isotopic reversals in deep basin gas: Evidence
844 for limits to the stability of hydrocarbons. *Org. Geochem*. **41**(12), 1285-1296.

845 Chacko T., Cole D.R. and Horita, J. (2001) Equilibrium oxygen, hydrogen and carbon isotopes fractionation
846 factors applicable to geologic systems. *Rev. Mineral. Geochem.* **43**, 1-81.

847 Chatellier J-Y., Ferworn K., Lazreg Larsen N., Ko S., Flek P., Molgat M. and Anderson I. (2013)
848 Overpressure in shale gas: when geochemistry and reservoir engineering data meet and agree. In *Critical*
849 *Assessment of Shale Resource Plays* (eds. J. Chatellier and D. Jarvie). *AAPG Memoir* **103**, 45–69.

850 Chatellier J.-Y. and Perez R. (2015) Review of traditional and new maturity indicators: differences and
851 complementarities. Search and Discovery Article #41654(abstr.).

852 Chatellier J.-Y., Simpson K., Perez R. and Tribovillard N. (2018) Geochemically focused integrated
853 approach to reveal reservoir characteristics linked to better Montney productivity potential. *Bull. Can. Pet.*
854 *Geol.* **66**(2), 516-551.

855 Chung H.M., Gormly J.R. and Squires R.M. (1988) Origin of gaseous hydrocarbons in subsurface
856 environments: theoretical considerations of carbon isotope distribution. *Chem. Geol.* **71**, 97-103.

857 Clayton C. (1991a) Carbon isotope fractionation during natural gas generation from kerogen. *Mar. Petrol.*
858 *Geol.* **8**, 232-240.

859 Clayton C.J. (1991b) Effect of maturity on carbon isotope ratios of oils and condensates. *Org. Geochem.*
860 **17**, 887-899.

Cole D.R. and Chakraborty S. (2000) Rates and mechanisms of isotope exchange. *Rev. Mineral. Geochem.* **43**, 83-233.

Dai J., Ni Y., Huang S., Gong D., Liu D., Feng Z., Peng W. and Han W. (2016) Secondary origin of negative carbon isotopic series in natural gas. *J. Nat. Gas Geosci.* **1**, 1-7.

Duffey G.H. (2013) Modern physical chemistry: a molecular approach. Springer Science and Business Media, New York, pp. 554.

Egbobawaye E.I. (2017) Petroleum source rock evaluation and hydrocarbon potential in Montney Formation unconventional reservoir, Northeastern British Columbia, Canada. *Nat. Resour.* **8**, 716-756.

Ellis L., Brown A., Schoell M. and Uchytil S. (2003) Mug gas isotope logging (MGIL) assists in oil and gas drilling operations. *Oil Gas J.* **101**(21), 32-41.

Faber E. (1987) Zur Isotopengeochemie gasf'ormiger Kohlenwasserstoffe. *Erdol, Erdgas & Kohle* **103** (H.5), 210-218.

Fan B., Wang X. and Shi L. (2018) Gas-desorption of low-maturity lacustrine shales, Triassic Yanchang Formation, Ordos Basin, China. *Open Geosci* **10**, 688-698.

Faiz M., Zoitsas A., Altmann C., Baruch E. and Close D. (2018) Compositional variations and carbon isotope reversal in coal and shale gases of the Bowenand Beetaloo basins, Australia. In *Application of analytical techniques to petroleum systems* (eds. Dowey P., Osborne M. and Volk H.). Geological Society, London, Special Publications, **484**.

Feng Z., Huang S., Wu W., Xie C., Peng W. and Cai, Y. (2017) Longmaxi shale gas geochemistry in changing and Fuling gas fields, the Sichuan Basin. *Energ. Explor. and Exploit.* **35**(2), 259-278.

Ferri F., Hayes M. and Nelson A. (2013) Liquids potential of the Lower to Middle Triassic Montney and Doig formations, British Columbia. In *Geoscience Reports 2013*. British Columbia Ministry of Natural Gas Development, pp. 1–11.

Gao B. (2016) Geochemical characteristics and geological significance of shale gas from the Lower Silurian Longmaxi Formation in Sichuan Basin, China. *J. Nat. Gas Geosci.* **1**, 119-129.

Gao L., Schimmelmann A., Tang Y. and Mastalerz M. (2014) Isotope rollover in shale gas observed in laboratory pyrolysis experiments: Insight to the role of water in thermogenesis of mature gas. *Org. Geochem.* **68**, 95-106.

Gai H., Tian H., Cheng P., Zhou Q., Li T., Wang X. and Xiao X. (2019) Influence of retained bitumen in oil-prone shales on the chemical and carbon isotopic compositions of natural gases: implications from pyrolysis experiments. *Mar. Petrol. Geol.* **101**, 148-161.

Hakami A., and Inan S. (2016). A basin modeling study of the Jafurah sub-Basin, Saudi Arabia: implications for unconventional hydrocarbon potential of the Jurassic Tuwaiq Mountain Formation. *Int. J. Coal Geol* **165**, 201-222.

Hakami A., Ellis L., Al-Ramadan K. and Abdelbagi S. (2016) Mud gas isotope logging application for sweet spot identification in an unconventional shale gas play: a case study from Jurassic carbonate source rocks in Jafurah Basin, Saudi Arabia. *Mar. Petrol. Geol.* **76**, 133-147.

Hao F. and Zou H. (2013) Cause of shale gas geochemical anomalies and mechanisms for gas enrichment and depletion in high-maturity shales. *Mar. Petrol. Geol.* **44**, 1-12.

Hayes J.M. (1993) Factors controlling ^{13}C contents of sedimentary organic compounds: principles and evidence. In *Marine Sediments, burial, pore water chemistry, microbiology and diagenesis* (eds. Parkes R.J., Westbroek P. and de Leeuw J.W.).. *Mar. Geol.* **113**, 111-125.

Heroux Y. and R. Bertrand (1991) Maturation thermique de la matière organique dans un bassin du Paléozoïque inférieur, basses-terres du Saint Laurent, Québec, Canada. *Can. J. Earth Sci.* **28**, 1019–1030.

Ibrahimbas A. and Riediger C. (2004) Hydrocarbon source rock potential as determined by rock-eval 6 / TOC pyrolysis, Northeast British Columbia and Northwest Alberta. In *Summary of activities Resource development and geoscience branch* (ed. Ferri, F.). British Columbia Ministry of Energy and Mines, pp. 7-18.

Jacob H. (1989) Classification, structure, genesis, and practical importance of natural solid bitumen ("migrabitumen"). *Int. J. Coal Geol.* **11**, 65–79.

James A.T. (1983) Correlation of natural gas by use of carbon isotopic distribution between hydrocarbon components. *Am. Assoc. Pet. Geol. Bull.* **67**(7), 1176-1191.

James A. T. (1990) Correlation of reservoired gases using the carbon isotopic compositions of wet gas components. *Am. Assoc. Pet. Geol. Bull.* **74**(9), 141-1458.

Janiga M., Kania M. and Matyasik I. (2015) The isotopic composition of gaseous hydrocarbons - tool for polish shale gas system evaluation. *Nafta-Gaz* **71**(6), 370-375.

Kaye J.A. (1992) Isotope Effects in gas-phase chemical reactions and photodissociation processes. In *Isotope Effects in gas-phase chemistry* (ed. Kaye J.A.). ACS Symposium Series **502**; American Chemical Society, pp. 1-14.

Kotarba M.J. and Nagao K. (2015) Molecular and isotopic compositions and origin of natural gases from Cambrian and Carboniferous-Lower Permian reservoirs of the onshore Polish Baltic region. *Int. J. Earth Sci.* **104**(1), 241-261.

Kuppe F., Haysom S. and Nevokshonoff G. (2012) Liquids rich unconventional Montney: the geology and the forecast. *Society of Petroleum Engineers*, **162824**.

Lavoie D., Pinet N., Dietrich J., Hannigan P., Castonguay S., Hamblin A.P. and Giles P. (2009) Petroleum resource assessment, Paleozoic successions of the St. Lawrence Platform and Appalachians of eastern Canada, *Geological Survey of Canada*, Open File **6174**.

Li X., Xiao X., Tang Y., Tian H., Zhou Q., Yang Y., Dong P., Wang Y. and Song, Z. (2008) The modeling of carbon isotope kinetics and its application to the evaluation of natural gas. *Front. Earth Sci-PRC* **2**(1), 96-104.

Liu C., Liu P., McGovern G.P. and Horita, J. (2019) Molecular and intermolecular isotope geochemistry of natural gases from the Woodford Shale, Arkoma Basin, Oklahoma. *Geochim. Cosmochim. Acta* **255**, 188-204.

Liu Q., Wu X., Wang X., Jin Z., Zhu D., Meng Q, Huang S., Liu J., and Fu Q. (2019) Carbon and hydrogen isotopes of methane, ethane, and propane: a review of genetic identification of natural gas. *Earth-Sci. Rev.* **190**, 246-272.

Lorant F., Prinzhofer A., Behar F. and Huc A-Y. (1998) Carbon isotopic and molecular constraints on the formation and the expulsion of thermogenic hydrocarbon gases. *Chem. Geol.* **147**, 249-264.

Mango F.D. and Jarvie D.M. (2009) Low-temperature gas from marine shales: wet gas to dry gas over experimental time. *Geochem. T.* **10**:10.

Mango F.D. and Jarvie D.M. (2010) Metathesis in the generation of low-temperature gas in marine shales. *Geochem. T.* **11**:1.

Mango F.D., Jarvie D.M. and Herriman E. (2009) Natural gas at thermodynamic equilibrium implications for the origin of natural gas. *Geochem. T.* **10**:6.

Mi J., Wang H., He K., Bai J. and Liu C. (2018) Demethylation as a mechanism for isotopic reversals of shale gas generated at overmaturity. *J. Anal. Appl. Pyrol.* **135**, 361-368.

Milkov A.V. and Etiope G. (2018) Revised genetic diagrams for natural gases based on a global dataset of >20,000 samples. *Org. Geochem.* **125**, 109-120.

National Energy Board (2013) *The ultimate potential for unconventional petroleum from the Montney Formation of British Columbia and Alberta*. Energy Briefing Note, Canada.

Ness S.M. (2001) *The application of basin analysis to the Triassic succession, Alberta Basin: an investigation of burial and thermal history and evolution of hydrocarbons in Triassic rocks* [unpublished master's thesis]. University of Calgary.

Ni Y., Gao J., Chen J., Liao F., Liu J. and Zhang D. (2018) Gas generation and its isotope composition during coal pyrolysis: Potential mechanism of isotope rollover. *Fuel* **231**, 387-395.

Norville G. (2014*) Isotope geochemistry of natural gas from the Horn River Basin: understanding gas origin storage and transport in an unconventional shale play* [unpublished Ph. D. Thesis]. University of Alberta.

Polyakov V.B. and Kharlashina N.N. (1994) Effect of pressure on equilibrium isotopic fractionation. *Geochim. Cosmochim. Acta* **58**, 4739-4750.

Prinzhofer A., and Huc A.Y. (1995) Genetic and post-genetic molecular and isotopic fractionations in natural gases. *Chem. Geol.* **126**, 281–290.

Qu Z., Sun J., Shi J., Zhan Z., Zou Y. and Peng P. (2016) Characteristics of stable carbon isotopic composition of shale gas. *J. Nat. Gas Geosci.* **1**, 147-155.

964 Repetski J.E., Ryder R.T., Weary D.J., Harris A.G. and Trippi M.H. (2008) Thermal maturity patterns (CAI
965 and $\%R_0$) in Upper Prdovician and Devonian rocks of the Appalachian Basin: a major revision of USGS
966 Map 1-917-E using new subsurface collection. *U.S. Geological Survey Scientific Investigations Map* **3006**.

967 Riediger C.L. (1990) Rock-Eval/TOC data from the Lower Jurassic "Nordegg Member", and the Lower
968 and Middle Triassic Doig and Montney formations, Western Canada Sedimentary Basin, Alberta and British
969 Columbia. *Geological Survey of Canada*, Open File **2308**.

970 Riediger C.L. (1997) Geochemistry of potential hydrocarbon source rocks of Triassic age in the Rocky
971 Mountain Foothills of Northeastern British Columbia and West-Central Alberta. *Bull. Can. Pet. Geol.* **45**,
972 719-741.

973 Rokosh C., Lyster S., Anderson A., Berhane H., Brazzoni T. Chen D., Cheng Y., Mack T, Pana C. and
974 Pawlowicz J. (2012) Summary of Alberta's shale- and siltstone-hosted hydrocarbon resource potential.
975 *Energy Resources Conservation Board / Alberta Geological Survey*, open file report **2012-06**.

976 Rooney M.A., Claypool G.E. and Chung, H.M. (1995) Modeling thermogenic gas generation using carbon
977 isotope ratios of natural gas hydrocarbons. *Chem. Geol.* **123**, 219-232.

978 Rowe D. and Muehlenbachs A. (1999) Low-temperature thermal generation of hydrocarbon gases in
979 shallow shales. *Nature* **398**, 61-63.

980 Schoell M. (1983) Genetic characterization of natural gases. *Am. Assoc. Pet. Geol. Bull.* **67**(12), 2225-2238.

981 Sereda R. (2017) The lower Montney Turbidite Complex of Northwest Alberta and Northeast British
982 Columbia: evolution of an oil and gas play from conventional to unconventional. Search Discovery Article
983 #10987(abstr.).

984 Sherwood Lollar B., Westgate T.D., Ward J.A., Slater G.F. and Lacrampe-Couloume G. (2002) Abiogenic
985 formation of alkanes in the Earth's crust as a minor source for global hydrocarbon reservoirs. *Nature* **416**,
986 522-524.

987 Sherwood Lollar B., Lacrampe-Couloume G., Slater G.F., Ward J.A., Moser D.P., Gihring T.M., Lin L.-H.
988 and Onstott T.C. (2006) Unravelling abiogenic and biogenic sources of methane in the Earth's deep
989 subsurface. *Chem. Geol.* **226**, 328-339.

990 Sherwood Lollar B., Lacrampe-Couloume G., Voglesonger K., Onstott T.C., Pratt L.M. and Slater G.F.
991 (2008) Isotopic signatures of CH4 and higher hydrocarbon gases from Precambrian Shield sites: A model
992 for abiogenic polymerization of hydrocarbons. *Geochim. Cosmochim. Acta* **72**, 4778-4795.

993 Tang Y., Perry J.K., Jenden and P.D. and Schoell, M. (2000) Mathematical medeling of stable carbon isotope
994 ratios in natural gases. *Geochim. Cosmochim. Acta* **64**(15), 2673-2687.

995 Thiagarajan N., Xie, H., Ponton C., Kitchen N., Peterson B., Lawson M., Formolo M., Xiao Y., and Eiler J.
996 (2020) Isotopic evidence for quasi-equilibrium chemistry in thermally mature natural gases. *PNAS* **117**(8),
997 3989-3995.

998 Tilley B. and Muehlenbachs K. (2006) Gas maturity and alteration systematics across the Western Canada
999 Sedimentary Basin from four mud gas isotope depth profiles. *Org. Geochem.* **37**, 1857-1868.

1000 Tilley B. and Muehlenbachs K. (2013) Isotope reversals and universal stages and trends of gas maturation
1001 in sealed, self-contained petroleum systems. *Chem. Geol.* **339**, 194-204.

1002 Tilley B., McLellan S., Hiebert S., Quartero B., Veilleux B. and Muehlenbachs, K. (2011) Gas isotope
1003 reversals in fracture gas reservoirs of the western Canadian Foothills: mature shale gases in disguise. *Am.*
1004 *Assoc. Pet. Geol. Bull.* **95** (8), 1399-1422.

1005 Troup A., Edwards S., Grigorescu M., Dixon O., Gopalakrishnan S. and McKillop M. (2018) The shale oil
1006 potential of the Toolebuc Formation, Eromanga and Carpentaria basins, Queensland: Data and
1007 interpretation. Queensland Geological Record **2018/01**.

1008 Whiticar M.J. (1990). A geochemical perspective of natural gas and atmospheric methane. *Org. Geochem.*
1009 **16**, 531–547.

1010 Whiticar M.J. (1994) Correlation of natural gases with their sources. In *The petroleum system from source*
1011 *to trap* (eds. Magoon L.B, and Dow W.G.). AAPG Memoir **60**, 261-284.

1012 Whiticar M.J. (1999) Carbon and hydrogen isotope systematics of bacterial formation and oxidation of
1013 methane. *Chem. Geol.* **161**, 291-314.

1014 Wood J. and Sanei H. (2016) Secondary migration and leakage of methane from a major tight-gas system.
1015 *Nat. Commun.* **7**(13614), 1-9.

1016 Wood J.M., Sanei H., Haeri-Ardakani O., Curtis M.E., Akai T. and Currie C. (2018) Solid bitumen in the
1017 Montney Formation: diagnostic petrographic characteristics and significance for hydrocarbon migration.
1018 *Int. J. Coal Geol.* **198**, 48-62.

1019 Wu Y., Zhang Z., Sun L., Li Y., Zhang M. and Ji L. (2019) Stable isotope reversal and evolution of gas during
1020 the hydrous pyrolysis of continental kerogen in source rocks under supercritical conditions. *Int. J. Coal*
1021 *Geol.* **205**, 105-114.

1022 Xia X., Chen J., Braun R. and Tang Y. (2012) Isotopic reversals with respect to maturity trends due to
1023 mixing of primary and secondary products in source rocks. *Chem. Geol.* **339**, 205-212.

1024 Xia X. and Gao Y. (2018) Depletion of ^{13}C in residual ethane and propane during thermal decomposition
1025 in sedimentary basins. *Org. Geochem.* **125**, 121-128.

1026 Zeng H., Li J. and Huo Q. (2013) A review of alkane gas geochemistry in the Xujiaweizi fault-depression,
1027 Songliao Basin. *Mar. Petrol. Geol.* **43**, 284-296.

1028 Zhang M., Tang Q., Cao C., Lv Z., Zhang T., Zhang D., Li Z. and Du L. (2018) Molecular and carbon
1029 isotopic variation in 3.5 years shale gas production from Longmaxi Formation in Sichuan Basin, China. *Mar.*
1030 *Petrol. Geol.* **89**, 27-37.

Zhang S., He K., Hu G., Mi J., Ma Q., Liu K. and Tang, Y. (2018) Unique chemical and isotopic characteristics and origins of natural gas in the Paleozoic marine formations in the Sichuan Basin, SW China: Isotope fractionation of deep and high mature carbonate reservoir gases. *Mar. Petrol. Geol.* **89**, 68-82.

Zhao J-Z., Li J., WU W-T., Cao Q., Bai Y-B, and Er C. (2019) The petroleum systems: a new classification scheme based on reservoir qualities. *Pet. Sci.* **16**, 229-251.

Zou Y.R., Cai Y.L., Zhang C.C., Zhang X. and Peng P.A. (2007) Variations of natural gas carbon isotope-type curves and their interpretation: a case study. *Org. Geochem.* **38**(8), 1398-1415.

Zumberge J., Ferworn K. and Brown S. (2012) Isotopic reversal ('rollover') in shale gases produced from the Mississippian Barnett and Fayetteville formations. *Mar. Petrol. Geol.* **31**, 43-52.

Figure captions

Figure 1. The location of the Montney Formation in Western Canada, its resource types, and the study area (rectangle). Modified after the National Energy Board (2013).

Figure 2. Methane, ethane and propane $\delta^{13}C$ profiles (a-d) and the corresponding $\Delta^{13}C_{C_1\text{-}C_2}$, $\Delta^{13}C_{C_2\text{-}C_3}$, and $\Delta^{13}C_{C_1\text{-}C_3}$ values (e-h) of samples from four wells from the Lorraine Shale, Quebec. Data from Chatellier et al. (2013). The wells are a,e) Fortierville, b,f) Leclercville, c,g) St. Edouard 1a, and d,h) St. Edouard 1.

Figure 3. Molecular and isotopic changes with increasing depth before and after the even isotopic distribution (EID) for samples from the wells (a) Fortierville and (b) Leclercville from the Lorraine shale, as indicated by: (c,d) the *iso*-butane to *n*-butane ratio iC_4/nC_4, (e,f) % mole distribution of C_1-C_3 alkanes as reported by Chatellier et al. (2013), (g,h) the C_2/C_3 ratio, (i,j) the $\delta^{13}C$ of ethane, and (k,l) the $\delta^{13}C$ of propane.

Figure 4. The $\Delta^{13}C_{C_1\text{-}C_2}$ versus $\Delta^{13}C_{C_1\text{-}C_3}$ plot for gas classification. Gas samples from low-permeability reservoirs around the world.

Figure 5. $\Delta^{13}C_{C_1\text{-}C_2}$ versus $\Delta^{13}C_{C_1\text{-}C_3}$ plot of samples from the Montney Formation, including produced gas data already published and other samples measured by the Applied Geochemistry Group (University of Calgary). For the Well A, the samples correspond to mud-gas except the indicated as wellhead.

Figure 6. Different isotopic fractionation models for (a) C_1-C_3 alkanes from natural gas at 1.5 $\%R_o$ including the Rayleigh model for labile kerogen and refractory kerogen (Clayton 1991a) and the isotope exchange model by James (1983), and (b) the EID from this study.

Figure 7. Gas samples from low-permeability reservoirs represented in a compound specific carbon isotopic analysis interpretation chart by Abrams (2017) after James (1983, 1990).

Figure 8. Equilibrium plot (modified after Mango et al., 2009) for samples from the Barnett Shale. The distinction of wet-gas samples versus dry-gas samples is based on Figure 4 and the EID. Q = $[(CH_4).(C_3H_8)]/[(C_2H_6)^2]$, using the vol % composition of the C_1-C_5 compounds in natural gas.

Figure 9. Prinzhofer and Huc diagram, modified after Lorant (1998) for (a) the Barnett Shale, USA (b) Pomeranian, Poland, and (c) Fortierville/Leclercville, Lorraine Shale, Canada.

Figure 10. Gas metathesis equilibrium factors $(CH_4).(C_3H_8)$ and $(C_2H_6)^2$ versus of the $\Delta^{13}C_{C_1\text{-}C_2}$ of Barnett Shale.

Figure 11. The $\Delta^{13}C_{C_1\text{-}C_2}$ versus $\Delta^{13}C_{C_1\text{-}C_3}$ plot for gas classification. Gas samples from the Woodford Shale in the SCOOP play. Data from Abrams and Thomas (2020).